Optimization of Laminated Composite Structures

Henrichsen, Søren Randrup

DOI (link to publication from Publisher):
10.5278/vbn.phd.engsci.00041

Publication date:
2015

Document Version
Publisher's PDF, also known as Version of record

OPTIMIZATION OF LAMINATED COMPOSITE STRUCTURES

BY
SØREN RANDRUP HENRICHSEN

DISSERTATION SUBMITTED 2015

AALBORG UNIVERSITY
DENMARK

Optimization of Laminated Composite Structures

Søren Randrup Henrichsen

Department of Mechanical and Manufacturing Engineering
Aalborg University, Denmark.

PhD Thesis

2015

Thesis submitted: November, 2015

PhD supervisors: Erik Lund, Prof., PhD, MSc
Department of Mechanical and Manufacturing Engineering,
Aalborg University, Denmark

Esben Lindgaard, Assoc. Prof., PhD, MSc
Department of Mechanical and Manufacturing Engineering,
Aalborg University, Denmark

PhD committee: Professor Sergey V. Sorokin (chairman)
Aalborg University

Head of Composites Group Eelco Luc Jansen
Leibniz Universität Hannover

Professor Jakob Søndergaard Jensen
Technical University of Denmark

PhD Series: Faculty of Engineering and Science, Aalborg University

ISSN (online): 2246-1248
ISBN (online): 978-87-7112-408-8

Published by:
Aalborg University Press
Skjernvej 4A, 2nd floor
DK – 9220 Aalborg Ø
Phone: +45 99407140
aauf@forlag.aau.dk
forlag.aau.dk

Printed in Denmark by Rosendahls, 2015

Preface

This thesis has been submitted to the Faculty of Engineering and Science at Aalborg University in partial fulfillment of the requirements for the degree of Doctor of Philosophy in Mechanical Engineering. The thesis is written as a collection of peer-reviewed papers as recommended by the Doctoral School of Engineering and Science. The PhD project was a part of the research project *FiberLab - The most advanced and cost effective fibre production unit in the world* (grant no. 107-2012-2 from The Danish National Advanced Technology Foundation (DNATF)) of which the main focus for Aalborg University was the development of efficient optimization methods. The research project was closed by DNATF May 2013, and the PhD project was carried on as an independent project focusing on buckling optimization of laminated composite structures.

The project was supervised by Erik Lund and Esben Lindgaard. I am very thankful for their competent guidance throughout the project and inspiring me to pursue my goals. During the PhD project I visited Paul Weaver at University of Bristol. I had a really good time and enjoyed our discussions wherever it was at the university, a pub, at football etc.

Last but not least, I would like to send my sincere gratitude to my fiance Runa for always being there for me, her joyful spirit, and reminding me to enjoy the little things in life.

Aalborg, November 2015

Søren Randrup Henrichsen

Abstract

Laminated composite materials are widely used in the design of light weight high performance structures like wind turbine blades and aeroplanes due to their superior stiffness and strength-to-weight-ratios compared to their metal counter parts. Furthermore, the use of laminated composite materials allows for a higher degree of tailoring of the resulting material. To enable better utilization of the composite materials, optimum design procedures can be used to assist the engineer. This PhD thesis is focused on developing numerical methods for optimization of laminated composite structures.

The first part of the thesis is intended as an aid to read the included papers. Initially the field of research is introduced and the performed research is motivated. Secondly, the state-of-the-art is reviewed. The review includes parameterizations of the constitutive properties, linear and geometrically non-linear analysis of structures, buckling and post-buckling analysis of structures, and formulations for optimization of structures considering stiffness, buckling, and post-buckling criteria. Lastly, descriptions, main findings, and conclusions of the papers are presented.

The papers forming the basis of the contributions of the PhD project are included in the second part of the thesis. Paper A presents a framework for free material optimization where commercially available finite element analysis software is used as analysis tool. Robust buckling optimization of laminated composite structures by including imperfections into the optimization process is the topic of Paper B. In Paper C the design sensitivities for asymptotic post-buckling optimization are derived. Furthermore, optimization formulations are introduced and demonstrated for optimum post-buckling design.

Dansk Resumé

Laminerede kompositte materialer er bredt anvendt til konstruktion af letvægtsstrukturer. Kompositte materialer anvendes for eksempel i vindmøllevinger og flyvemaskiner grundet overlegen styrke og stivhed til vægt forhold sammenlignet med letvægtsmetaller. Anvendelse af kompositter giver muligheden for at skræddersy det endelige materiale, hvormed effektive strukturer kan konstrueres. For at muliggøre bedre udnyttelse af kompositmaterialerne kan optimale designprocedurer anvendes. Fokus i denne ph.d. afhandling er at udvikle numeriske metoder til optimering af laminerede kompositkonstruktioner.

Den første del af afhandlingen er en hjælp til at læse de medfølgende artikler. Først introduceres forskningsområdet, ligesom den udførte forskning motiveres. Derefter præsenteres et litteraturstudie, hvor den nyeste viden indenfor parameterisering af kompositmaterialer, lineær og ikke-lineær analyse af strukturer, bulings- og postbulingsanalyse samt optimering af strukturer med stivheds-, bulings- og postbulingskriterier er inkluderet. Slutteligt introduceres artiklerne, hvor indholdet, de vigtigste resultater og konklusionerne præsenteres.

Artiklerne, som danner grundlaget for ph.d. projektet, er inkluderet i anden del af afhandlingen. Artikel A omhandler free material optimization, hvor et kommercielt tilgængeligt elementmetodeprogram benyttes som analyseværktøj. Robust bulingsoptimering af laminerede kompositkonstruktioner er udført i Artikel B. Robust optimering opnås ved at inkludere imperfektioner i optimeringsprocessen. I Artikel C udledes designfølsomhederne for asymptotisk postbulingsoptimering. Ligeledes introduceres en række optimeringsformuleringer og effekten af disse formuleringer demonstreres.

Thesis Details

This thesis is made as a collection of papers and consists of an introduction to the area of research and three papers for publication in refereed scientific journals of which two are accepted and one is submitted in initial form.

Thesis Title:	Optimization of Laminated Composite Structures
PhD Student:	Søren Randrup Henrichsen
PhD Supervisors:	Erik Lund, Prof., PhD, MSc Department of Mechanical and Manufacturing Engineering, Aalborg University, Denmark
	Esben Lindgaard, Assoc. Prof., PhD, MSc Department of Mechanical and Manufacturing Engineering, Aalborg University, Denmark

Publications in refereed journals

A) Henrichsen, S.R., Lindgaard, E., Lund, E. 2015. Free material stiffness design of laminated composite structures using commercial finite element analysis codes, *Structural and Multidisciplinary Optimization*, **51**(5), pp. 1097–1111.

B) Henrichsen, S.R., Lindgaard, E., Lund, E. 2015. Robust buckling optimization of laminated composite structures using discrete material optimization considering "worst" shape imperfections, *Thin-Walled Structures*, **94**, pp. 624–635.

C) Henrichsen, S.R., Weaver, P.M., Lindgaard, E., Lund, E. 2015. Post-buckling optimization of composite structures using Koiter's method, submitted to: *International Journal for Numerical Methods in Engineering*.

Publications in proceedings with review

D) Henrichsen, S.R., Lindgaard, E., Lund, E. (2015): Discrete material buckling optimization of laminated composite structures considering "worst" shape imperfections. *In: Proc. 3rd Int. Conference on Buckling and Postbuckling Behaviour of Composite Laminated Shell Structures*, Braunschweig, Germany, March 25–27 2015, 4 pages.

E) Henrichsen, S.R., Lindgaard, E., Lund, E. (2014): Buckling optimization of composite structures using a discrete material parametrization considering "worst" shape imperfections. *In: Proc. of 11th World Congress on Computational*

Mechanics (WCCM XI), 5th European Conference on Computational Mechanics (ECCM V), 6th European Conference on Computational Fluid Dynamics (ECFDVI) (eds. E. Onate, X. Oliver, A. Huerta), July 20–25, 2014, 2 pages.

F) Henrichsen, S.R., Lindgaard, E., Lund, E. (2013): Comparison of FMO, DMO, and CFAO for laminated composite structures. *In: Proc. 10th World Congress on Structural and Multidisciplinary Optimization*, Orlando, Florida, USA, May 19–24 2013, 1 page.

This thesis has been submitted for assessment in partial fulfillment of the PhD degree. The thesis is based on the submitted or published scientific papers which are listed above. Parts of the papers are used directly or indirectly in the extended summary of the thesis. As part of the assessment, co-author statements have been made available to the assessment committee and are also available at the Faculty. The thesis is not in its present form acceptable for open publication but only in limited and closed circulation as copyright may not be ensured.

Contents

Chapter 1

Introduction to the PhD project

In this chapter a short introduction to the PhD project, the field of research, and the objectives are given. The chapter serves as an introduction to the field of research and the choices made during the PhD period. This provides an overview of the background for the topics covered within the PhD project.

1.1 The PhD project

The PhD study was started as a part of the research project *FiberLab - The most advanced and cost effective fibre production unit in the world* sponsored by the Danish National Advanced Technology Foundation (DNATF). Besides Aalborg University, the project partners constituted the public research institutions; Technical University of Denmark and University of Southern Denmark and the private companies; DESMI, EL-BO, Eltronic, and Danish Technological Institute. The overall purpose of the project was to develop a robot-based composite manufacturing cell for complex-shaped products e.g., pump housings. The role of Aalborg University was to develop efficient optimization methods using commercial available Finite Element Analysis codes for the manufacturing cell. The PhD project was initialized within this topic, and the findings hereof are collected in Paper A. However, in May 2013 DNATF decided to close down the research project. This removed all obligations concerning the research topics within the PhD project.

After the FiberLab project was terminated, the PhD study was continued as an independent research project and the topic of the project was changed into buckling optimization of laminated composite structures. The change in topic was driven by two main factors:

- Since no partners remained in the project, the manufacturing cell would not be realized, and thus the back-bone of the initial research had been removed. Consequently, future findings would be somewhat artificial, as these could not be demonstrated on the manufacturing cell.

- Through meetings between the supervisors and PhD student, several interesting research topics within buckling optimization were identified, and it was decided to continue the PhD studies within this topic.

The outcome of the research within buckling optimization of laminated composite structures is collected in Paper B and Paper C, where a paper in robust buckling optimal design (Paper B) and a paper in asymptotic post-buckling optimization (Paper C) are presented.

1.2 Laminated composite materials

Composite materials are defined as materials which consist of two or more macroscopically distinct phases. This is different from e.g., alloy steel where the alloying materials are embedded in the microscopic scale, resulting in a material which appears macroscopically homogeneous. The most common example of a composite material is concrete, where particles of sand and gravel are bonded with a mixture of cement and water, hereby forming the resulting composite material [1]. In this work composite materials refer to fiber reinforced polymers (FRP's). FRP's consist of strong and stiff fibers e.g., glass fibers and carbon fibers, embedded in a light and compliant matrix e.g., epoxy [1], such that the resulting composite material features the best of both. The mechanical properties of composite materials are mainly governed by the fibers. Thus the high stiffness and strength properties are present in the fiber direction.

Laminates are manufactured by stacking and curing a number of plies. Figure 1.1 illustrates a five layered laminate where all plies have the same thickness. Mat A represents a FRP. Since the mechanical properties are dominated by the fibers, the orientation of the fibers within the ply must be specified. In the figure Mat B is an isotropic material hence no orientation is required as the mechanical properties are independent of orientation. The mechanical properties of a laminate are determined by several factors including material properties of each individual ply, the number of plies, the thickness of each ply, and the ply orientation. Consequently, the use of laminated composite

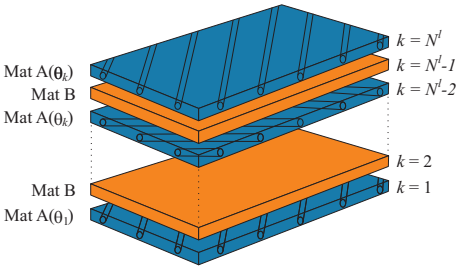

Figure 1.1: Exploded view of a laminate manufactured by stacking and curing a number of plies. Mat A represents a FRP with the fiber orientation θ, whereas Mat B is an isotropic material.

materials enables a large design freedom and a high degree of tailoring of the composite structure, and by careful design effective structures can be achieved, as the fibers can be placed and oriented such that the structure only possess stiffness to resist the operational requirements.

Composite materials are often used in high performance structures due to their superior stiffness and strength-to-weight-ratio compared to their metal counter parts. The high specific properties enable further weight reduction, which for e.g., civilian air transport results in reduced fuel consumption [2]. Typical applications of laminated composite materials are given in Figure 1.2. It is a common feature of the structures that the mass of the structure influences the performance of the structure like increased fuel consumption, larger forces transmitted through the structure etc.

Figure 1.2: Applications of laminated composite materials. Courtesy of Airbus, Wikipedia, Ferrari, Titleist, Siemens, European Space Agency, and LM Wind Power

1.3 Buckling and post-buckling of laminated composite structures

Structures loaded in tension primarily fail due to material failure. However, when a structure is loaded in compression, the structure may fail due to buckling prior to material failure. Buckling is a phenomenon where the configuration of a structure looses its stability and transforms to a secondary configuration called the buckled configuration. Considering a straight slender column, the stability can be tested by the method shown in Figure 1.3. The first step is to apply load to the column, this shortens the column. The straight column is the so-called pre-buckling configuration. At a fixed load level, a small disturbance may be applied to the column e.g., a small sideways displacement. After removal of the disturbance, one may define and evaluate stability. If the column returns to the straight configuration it is stable for the given load level, however, if the column transforms into a secondary, buckled, configuration it is unstable, and in this case the buckled configuration is a curved shape. Figure 1.4 presents a graphical description of the buckling phenomenon. Considering the left most figure, buckling of the column can be explained. As the structure is loaded it follows the fundamental equilibrium curve where the straight configuration is stable, and a small perturbation will not cause transformation into the buckled shape. This part is called the pre-buckling regime. At a certain load level, the fundamental equilibrium curve is crossed by a secondary equilibrium curve causing the straight configuration to loose its stability, this is called the critical point - or bifurcation point. At load levels above the critical load, the straight configuration remains an equilibrium configuration shown by the broken line in Figure 1.4, however it is unstable meaning that a small disturbance will cause the structure to switch from the unstable fundamental path to the stable secondary path where the column is curved. The response after the critical point is called the post-buckling regime as the structure is in its buckled configuration.

Different types of instability exist, and in this work two kinds of instabilities are considered namely bifurcation instability and limit point instability. In bifurcation type instability the fundamental equilibrium path is crossed by a secondary equilibrium path causing the fundamental path to loose its stability. This is represented by the left and center graphs in Figure 1.4. Limit point instability is caused by the fundamental equilibrium path loosing its stability without the crossing of a secondary equilibrium curve, and it is given by the right most graph in Figure 1.4. Besides the load at which a structure buckles, the response after buckling is of fundamental interest to the analyst. The post-buckling response reveals whether a structure is capable of carrying a load level above the critical point in its buckled configuration. If the buckled structure is capable of carrying load above the critical point at a configuration close to the unbuckled it is post-buckling stable, if not it is post-buckling unstable. Bifurcation type instabilities may or may not be post-buckling stable, whereas limit point instabilities always are unstable under load control, meaning that

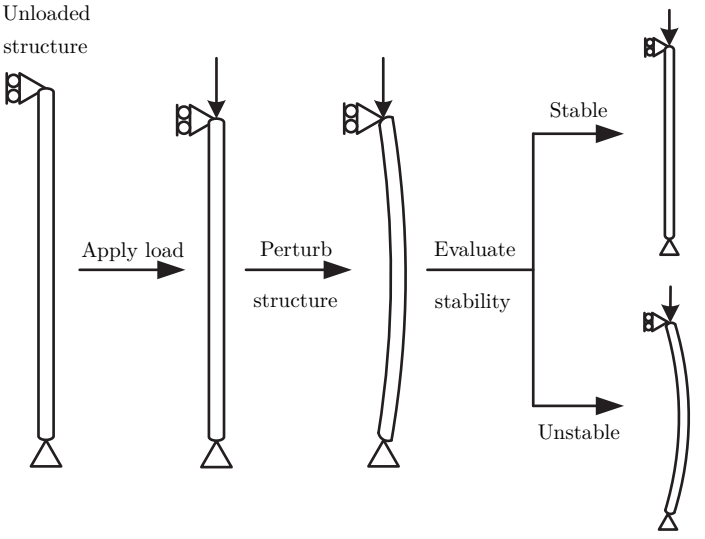

Figure 1.3: Buckling of a column. In the pre-buckling regime the column is in its straight pre-buckled configuration. To evaluate the stability a small perturbation is assigned to the column. If the column returns to the straight configuration after the perturbation is removed the structure is stable, if not the structure is unstable.

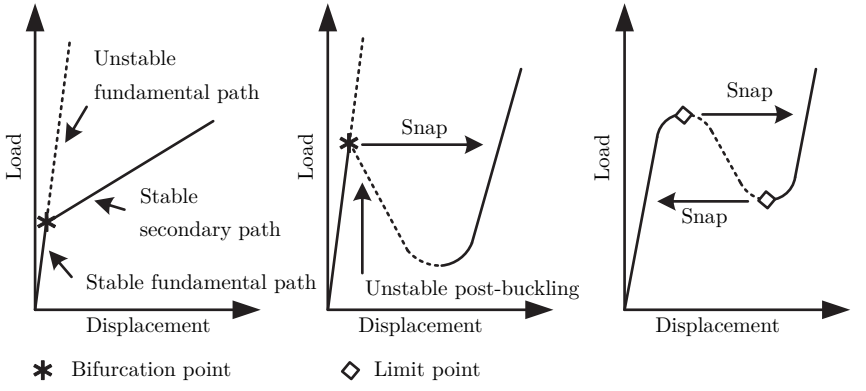

Figure 1.4: Various kinds of instabilities. The left and center figures represent bifurcation buckling with stable and unstable initial post-buckling, respectively. The right figure represents a limit point instability. Broken lines represent unstable equilibrium curves and solid lines stable equilibrium curves. If the post-buckling response is unstable the structure performs a snap when the load is increased marginally above the critical load, resulting in finite displacements.

Figure 1.5: Glider plane making a tight turn. Clear buckles are present on the wings. Photograph courtesy of Connie Indrebo.

the load is incremented, and the corresponding displacements are determined. If the post-buckling response is unstable, the structure exhibits a so-called snap where an infinitesimal increase in load causes a finite deformation of the structure due to the lack of adjacent stable equilibrium configurations [3].

For thin-walled structures buckling is an important design criterion. Considering the glider plane in Figure 1.5 clear buckling patterns are visible on the wings. It clarifies the need for analysis and design tools for structures operating around the buckling load. Buckling design tools for composite structures have a great potential for optimizing both the pre-buckling and post-buckling response as well as changing the critical load. Considering a square simply supported single layered composite plate subject to compression, the capabilities to tailor the buckling properties can be shown. By aligning the fibers in the loading direction the stiffness towards the loading is maximized, and by aligning the fibers at 45° the buckling load is maximized, see Figure 1.6 and 1.7 for the load - end shortening response and load - out-of-plane response, respectively. Furthermore, the 0° fibers possess more stiffness in the post-buckling regime compared to the 45° case, revealing the potential for performing both buckling load optimization and post-buckling optimization.

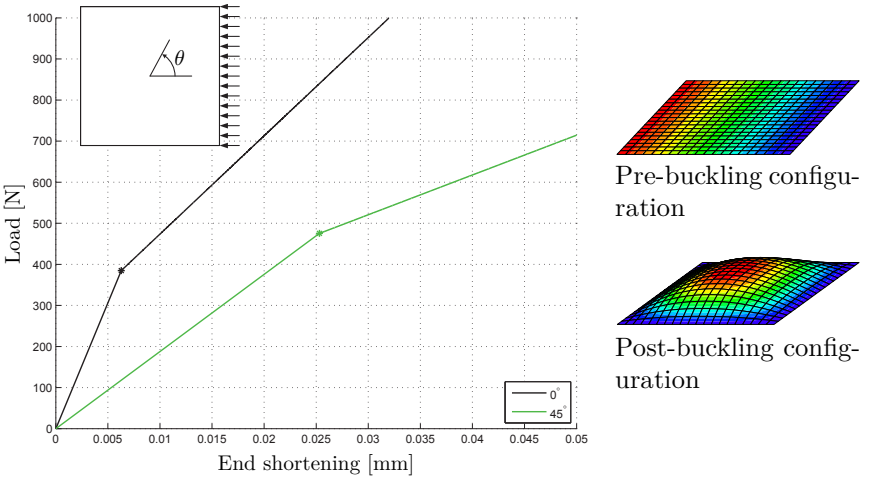

Figure 1.6: Load - end shortening response of the plate. The plate is in its flat pre-buckling configuration until the bifurcation point marked with an asterisk, whereafter it buckles with a single wave. The plate has a side length of 1 [m] and a thickness of 2 [mm].

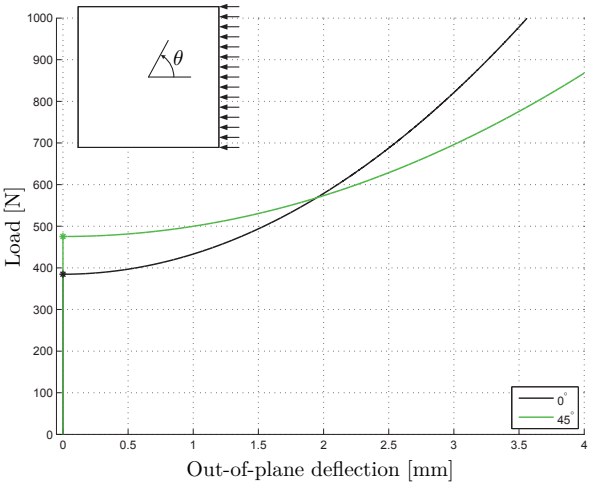

Figure 1.7: Load - out-of-plane deflection response of the plate. The plate has a side length of 1 [m] and a thickness of 2 [mm].

1.3.1 The role of imperfections

During manufacturing and operation of a structure deviations from the idealized structure and operation conditions are introduced. These deviations are defined as imperfections and can emerge from discrepancies in material properties, imperfect geometry of the structure, load misalignments etc. A famous example of an imperfect structure is the Leaning Tower of Pisa which has a visible geometric imperfection, see Figure 1.8. Consequently, it is important to assess the effect of the imperfections on the structural response. Considering the plate from the previous section, an imperfection corresponding to the first buckling mode shape can be applied, and by varying the amplitude, ξ, the effect of the imperfection can be determined. The nonlinear responses are given in Figure 1.9 and 1.10 for the end shortening and the out-of-plane deflection, respectively. It is immediately seen that the bifurcation point is not defined, and the load-displacement response is smooth. Additionally, the equilibrium curve is stable throughout the analysis, and the structure does not display any stability point. This is a consequence of the stable post-buckling response. Furthermore, for small imperfection amplitudes the perfect and imperfect equilibrium curves are almost coincident, and close to the critical point of the perfect structure the out-of-plane deflections for the imperfect structure are amplified.

If a simply supported cylindrical panel is considered instead of the plate, a structure with a highly unstable initial post-buckling response is obtained. Applying an imperfection corresponding to the first buckling mode shape the effect of the imperfection can be evaluated. The load - end shortening responses for various imperfection amplitudes are given in Figure 1.11. The buckling load

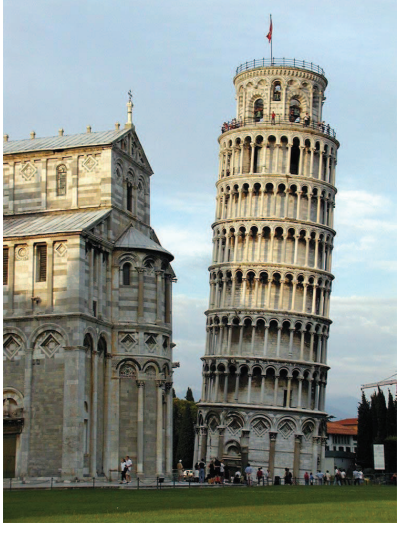

Figure 1.8: The Leaning Tower of Pisa. Photograph from Wikipedia.

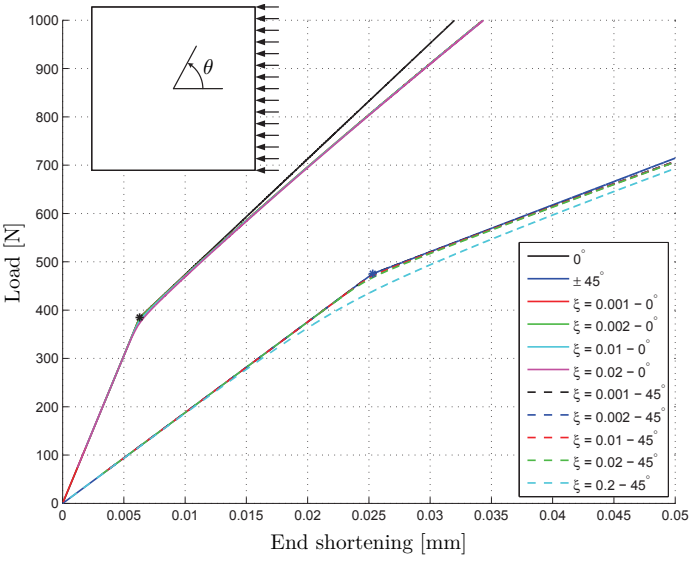

Figure 1.9: Load - end shortening response of the plate for various imperfection amplitudes, ξ, given in [mm] and different fiber angles θ. The plate has a side length of 1 [m] and a thickness of 2 [mm].

decreases with an increased imperfection amplitude, until the size of the imperfection amplitude is large such that the unstable part of the equilibrium curve is removed. Furthermore, the bifurcation instability for the perfect structure is replaced by a limit point instability for the imperfect structure. This effect along with the vanishing of the bifurcation point for the plate show that imposing imperfections is an effective way to eliminate the crossing of equilibrium curves and replace them with a single equilibrium curve.

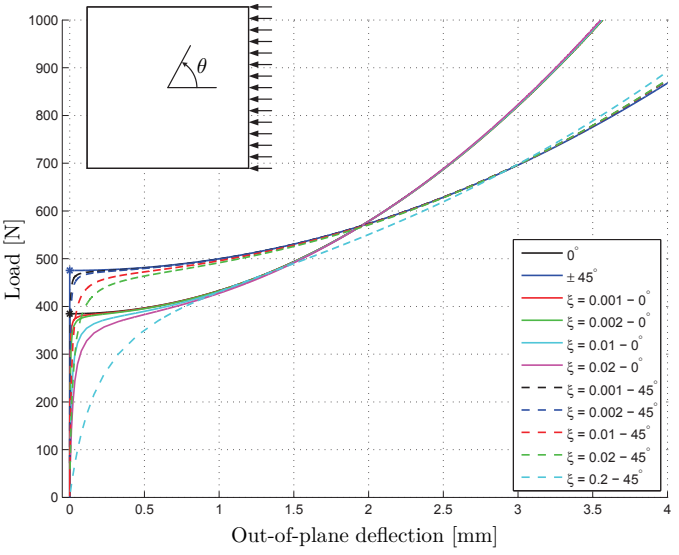

Figure 1.10: Load - out-of-plane deflection response of the plate for various imperfection amplitudes, ξ, given in [mm] and different fiber angles θ. The plate has a side length of 1 [m] and a thickness of 2 [mm].

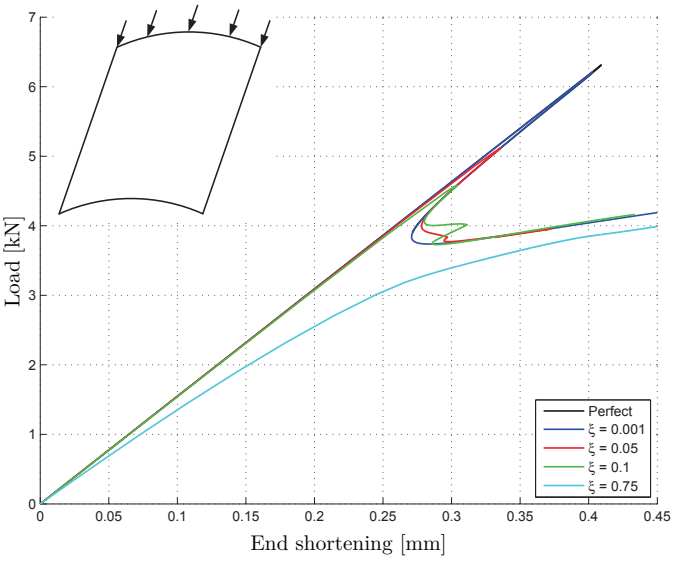

Figure 1.11: The load - end shortening response of the cylindrical panel for various imperfection amplitudes, ξ, given in [mm]. The fibers are aligned with the direction of the load. The panel is 245 [mm] wide, 500 [mm] long, and 1 [mm] thick.

Comparing the effect of imperfections for the cylindrical panel and the plate, it is seen that applying imperfections has a large effect on the response of the structure, and thus optimization methods where imperfections are taken into account are necessary. Additionally, the correlation between imperfection sensitivity and post-buckling stability is clarified, where post-buckling unstable structures are more sensitive towards imperfections than post-buckling stable structures.

1.4 Design and optimization of laminated composite structures

Proper design of laminated composite structures is a far from simple task. Application of composite materials introduces many design variables since properties like material, thickness, orientation etc., for each individual ply must be specified throughout the structure. Furthermore, the analysis models are often large and many design criteria are present e.g., mass, stiffness, and buckling. The common design approach is to update the design based on engineering knowledge and heuristics, which may result in inefficient and suboptimal designs. Effectively, rational analysis and design methods to assist the engineer during the design of laminated composite structures are desired. Application of optimum design procedures introduces an automated and rational analysis and design process, where the design is improved based on a performance measure describing the quality of the optimized structure. By continuously analyzing and improving the design of the structure the optimal structure which fulfills the operational requirements is obtained.

1.5 Objectives of the PhD project

The objective of the PhD study is to develop finite element analysis based methods for optimization of laminated composite structures, particulary with regard to stiffness, buckling and post-buckling criteria. The primary topics for investigation are:

- Effective optimization methods which can be combined with commercial finite element analysis software.
- Robust buckling optimal structures by handling imperfections.
- Post-buckling optimization of laminated composite structures.

These topics stem partly from the FiberLab project, partly from the desire to design even lighter composite structures which requires further knowledge concerning the buckling and post-buckling response of structures.

Chapter 2

State-of-the-art

This chapter presents an overview of the field of research, and serves as an aid to read the papers. The chapter covers the parameterizations, applied analysis methods, and optimization methods within the included papers. The PhD work is performed within a finite element framework to enable the possibility of analyzing general structures. Consequently, the equations are presented using a finite element notation, except for the post-buckling analysis, which easily is derived using the so-called Budiansky-Hutchinson notation, and afterwards is translated into a finite element notation.

The applied optimization formulations are based on optimizing the constitutive properties of the laminate, thus the chapter is initialized with a presentation of the applied parameterizations. Afterwards, linear finite element analysis and compliance optimization are covered. This forms the basis for the contributions in Paper A. Paper B concerns robust buckling optimization thus linear and geometrically nonlinear buckling analysis are reviewed. This is followed by design sensitivity analysis and robust buckling optimization by inclusion of imperfections. The last part of the chapter is concerned the derivation of the equations needed to perform asymptotic post-buckling analysis along with considerations concerning optimization of the post-buckling response, which is the topic of Paper C.

2.1 Parametrization of constitutive properties

The optimization formulations used in this work are based on optimizing the constitutive properties within the structure. In the papers three different constitutive parameterizations are used; Continuous Fiber Angle Optimization (CFAO), Free Material Optimization (FMO), and Discrete Material Optimization (DMO). The review is limited to these parameterizations. This however, only covers a subset of parameterizations for laminated composites, and for a comprehensive review of different parameterizations, refer to [4, 5].

2.1.1 Continuous Fiber Angle Optimization

Continuous Fiber Angle Optimization (CFAO) is concerned with the optimum orientation of an orthotropic material. In the general formulation, only the orientations, θ, are used as design variables. Thus no change in topology is possible. Optimal orientation of orthotropic materials is considered in [6], where the optimum angle for orthotropic materials with high and low shear stiffness is derived. The bounds on the elastic energy for an orthotropic material assuming a constant strain field are derived in [7], hereby showing the extremum angles and whether it is a minimum or maximum.

CFAO suffers from non-convexity as the orientation enters the constitutive tensor through trigonometric functions, see Eq. (2.1). However, with proper initial angles and move limit strategy optimum designs with good performance are obtained.

$$\begin{aligned} \mathbf{E}_{pl}(\theta_{pl}) &= \mathbf{T}(\theta_{pl})^{-1}\mathbf{E}\mathbf{T}(\theta_{pl})^{-T}, \quad \forall\, p, l \\ \mathbf{T}(\theta) &= \begin{bmatrix} c^2 & s^2 & 2sc \\ s^2 & c^2 & -2sc \\ -sc & sc & c^2 - s^2 \end{bmatrix}, \quad c = \cos(\theta),\ s = \sin(\theta) \end{aligned} \tag{2.1}$$

Here p is the patch and l is the layer. A patch defines a group of elements which are forced to have the same laminate layup properties. When optimizing using CFAO, it is important to secure that the bounds on the design variables never are reached, as this will have an effect on the remaining fiber angles. A good estimate for the bounds on the fiber angles are: $\theta_{\text{init}} \pm 180.9°$, where θ_{init} is the initial angle.

2.1.2 Free Material Optimization

Determination of the optimum material throughout a structure provides valuable information concerning e.g., the principal loading directions within a structure. Designing the optimum material among all existing and nonexisting materials is called Free Material Optimization (FMO). In FMO the only restrictions imposed on the material properties are that the resulting constitutive tensor is symmetric and positive semi-definite. Within these restrictions the optimum material among all materials is determined, and thus the results emerging from FMO define the best possible performance of a structure, which can be used to evaluate the quality of the results from other optimization methods.

The early work within FMO was conducted in [8–11] where [8] used the entries in the full symmetric constitutive matrix as design variables resulting in 6 design variables for 2D problems per design domain. Refs. [9–11] showed that the optimum free material is orthotropic with the principal material directions aligned and scaled with respect to the principal strains. Free Material Optimization is primarily demonstrated for mass constrained stiffness optimization where the amount of material is controlled by the trace of the constitutive tensor. Ref. [12] provides an overview of the results obtained through the PLATO-N project where the focus was to develop semi-definite programming

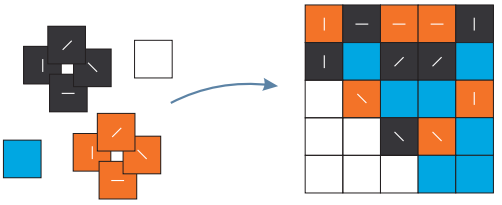

Figure 2.1: Schematic description of the Discrete Material Optimization approach. Each color represents a different material, where blue and white are isotropic materials or void and black and orange are orthotropic materials having different orientations. A total of 10 candidate materials are defined in the figure.

methods applicable for FMO and formulations for compliance and stress criteria are presented.

The resulting material is most likely not a physical available material, since no restrictions on the availability are imposed. FMO can be used to determine the optimum material properties throughout the structure. This optimized design can form the basis for a subsequent interpretation into a physical material. This has been attempted in [13] where an initial FMO design is post-processed by fiber paths for manufacturing using automated fiber placement.

2.1.3 Discrete Material Optimization

Discrete Material Optimization (DMO) is in essence a generalization of the multiphase topology optimization approach developed in [14]. A number of candidate materials, with orientations, are defined in the DMO approach. The task is to select the optimum among the available candidate materials, see Figure 2.1. The DMO approach represents a manufacturing process where the engineer has "a catalogue of different materials and orientations" from which the laminated composite structure is designed.

The DMO problem represents in principle a large combinatorial problem, but [15, 16] proposed a continuous relaxation with penalization of the integer problem, given by

$$\begin{aligned} \mathbf{E}_{pl}(x_{plc}) = & \sum_{c=1}^{n^c} w(x_{plc})\mathbf{E}_c, \quad \forall\, p, l \\ x_{plc} \in & \;]0,1[\end{aligned} \tag{2.2}$$

Here $\mathbf{E}_{pl}$ is the constitutive matrix for patch p and layer l. $\mathbf{E}_c$ contains the constitutive properties for candidate c and the total number of candidate materials is n^c. w is the weight function, and suggestions for the penalization scheme are given in [15]. Lastly, x_{plc} are the design variables which have a similar meaning as for topology optimization i.e., $x_{plc} = 0$ means that the candidate material is not selected, whereas $x_{plc} = 1$ represents a selected candidate material. Only a single material can be selected in each design domain, and intermediate values

define an artificial pseudo-material. In the original formulation the weight functions are self-balancing and thus the design variables are coupled. Ref. [17, 18] proposed the multiphase SIMP (Solid Isotropic Material with Penalization) and multiphase RAMP (Rational Approximation of Material Properties) schemes which decouple the design variables. The proposed schemes are generalizations of the single isotropic material versions of the SIMP and RAMP schemes, see e.g., [19–21]. The multiphase SIMP formulation is given as

$$\begin{aligned} \mathbf{E}_{pl}(x_{plc}) &= \mathbf{E}_0 + \sum_{c=1}^{n^c} x_{plc}^q \mathbf{E}_c, \quad q \geq 1, \quad \forall\, p, l \\ x_{plc} &\in [0, 1] \\ \sum_{c=1}^{n^c} x_{plc} &= 1, \quad \forall\, p, l \end{aligned} \tag{2.3}$$

Here $\mathbf{E}_0$ is a weak material securing positive definiteness of the constitutive tensor, and q is the penalization factor. The formulation results in a large number of sparse linear constraints in the optimization problem, and thus an optimizer which efficiently can handle these is required. This formulation and the equivalent multiphase RAMP formulation have been used throughout this work. The DMO approach has successfully been applied to optimize structures with several criteria functions and a large number of design variables, see [22, 23].

The DMO approach results in a large number of design variables as one design variable per candidate material per layer per patch is needed. To reduce the number of design variables, Shape Functions with Penalization (SFP) and Bi-value Coding Parametrization (BCP) were introduced in [24, 25], respectively. SFP can be regarded as a special case of BCP where each candidate material is given a unique coding, hereby the number of design variables only scales logarithmic with the number of candidate materials.

2.2 Linear analysis of structures

When a structure is loaded it deforms, hereby internal forces develop which equilibrate the externally applied loads. The basics in static finite element analysis is to determine the displacement field which establish the equilibrium. If the response is assumed linear then the problem of obtaining the displacements can be solved directly. The linear static problem is given on finite element form as

$$\mathbf{K}_0\mathbf{D} = \mathbf{R} \tag{2.4}$$

Here $\mathbf{K}_0$ is the linear stiffness matrix, $\mathbf{D}$ is the global displacement vector, and $\mathbf{R}$ is the applied load vector. Eq. (2.4) is only applicable when the displacements, rotations, and strains are small.

2.3 Compliance optimization

Minimum compliance, or equivalently maximum stiffness, design is a standard optimization problem found many places in literature [19]. In Paper A it is used to demonstrate the applied free material optimization approach. The minimum compliance formulation applied in this work is based on the work by [26] which is a free material optimization parametrization based on the work by [9]. The formulation in [9] is changed from a stiffness distribution problem into a material distribution problem as

$$\underbrace{\mathbf{E}(x) = E(x)\boldsymbol{\alpha}_{xy}}_{\text{Formulation from ref. [9]}} \quad \Rightarrow \quad \underbrace{\mathbf{E}(x) = w(x)\overline{E}\boldsymbol{\alpha}_{xy}}_{\text{Formulation from ref. [26]}} \tag{2.5}$$

Here x contains the design variables. The method in [26] resembles a topology optimization approach where $\overline{E}$ is the maximum allowable stiffness and w is the weight function defined in a similar manner as in topology optimization. The anisotropy is defined by the principal strain directions and are collected in the $\boldsymbol{\alpha}_{12}$-matrix

$$\boldsymbol{\alpha}_{12} = \frac{1}{\epsilon_1^2 + \epsilon_2^2}\begin{bmatrix} \epsilon_1^2 & \epsilon_1\epsilon_2 & 0 \\ \epsilon_1\epsilon_2 & \epsilon_2^2 & 0 \\ 0 & 0 & 0 \end{bmatrix} \tag{2.6}$$

Here $\boldsymbol{\alpha}_{12}$ is defined in the local material coordinate system. ϵ_1 and ϵ_2 are the principal strains with $\epsilon_1 \geq \epsilon_2$. $\boldsymbol{\alpha}_{12}$ is rotated into the structural coordinate system to obtain $\boldsymbol{\alpha}_{xy}$. The reformulation by [26] provides the advantage that the amount of material is explicitly controlled compared to the formulation in [9] where the material constraint is implicitly controlled through the constraint on the amount of available stiffness.

2.4 Analysis of buckling

As described in section 1.3, the initial configuration for a slender structure loaded in compression will at a given load level become unstable, and the structure deforms into a secondary, buckled, configuration. Buckling is a consequence of a transition from a stable through a neutral stable into an unstable equilibrium configuration of the fundamental equilibrium curve. The stability of a system can be determined by the definiteness of the tangent stiffness matrix, $\mathbf{K}_T$. A pre-buckling equilibrium configuration has a positive definite tangent stiffness matrix, at the critical point $\mathbf{K}_T$ is positive semi-definite, and it is indefinite at an unstable configuration [3, 27].

When performing buckling analysis, the analyst searches for the loads at which the structure becomes unstable, the buckling load, and the associated buckling mode shape, $\boldsymbol{\phi}$. The stiffness matrix is singular at a critical point, and thus a non-zero vector, $\boldsymbol{\phi}$, exists which solves the equation

$$\mathbf{K}_T^c\boldsymbol{\phi} = \mathbf{0} \quad \text{thus} \quad \det\left(\mathbf{K}_T^c\right) = 0 \tag{2.7}$$

Here a superscript ^{c} defines the load and displacement configuration at the critical point of the structure. The lowest (positive) load factor is of primary interest in buckling analysis. The properties given in Eq. (2.7) are used when formulating the buckling problem. Initially geometrically nonlinear static analysis is presented, as the displacement field at the critical point is required to formulate the buckling problem.

2.4.1 Geometrically nonlinear analysis of structures

To perform a geometrically nonlinear (GNL) analysis a body in equilibrium is considered. For a body in equilibrium the residual $\mathbf{P}$ between the inner forces, $\mathbf{F}$, and the outer forces, $\mathbf{R}$, must be zero

$$\mathbf{P}(\mathbf{D},\mathbf{R}) = \mathbf{F}(\mathbf{D}) - \mathbf{R} = \mathbf{0} \tag{2.8}$$

The applied loads are assumed being conservative, thus are independent of the displacement. Eq. (2.8) represents a set of nonlinear equations used to determine the displacements between the unloaded and the loaded structure. To solve the equilibrium equations, the applied force is split up into a series of load steps $n = 1, 2, \ldots$. Each load step is solved using an iterative process. Assume that the structure is in equilibrium at load step $n-1$ and the equilibrium configuration in load step n is to be determined. To establish equilibrium, the residual is linearized and the incremental displacements $\delta\mathbf{D}_i^n$ which equilibrate the linearized problem are determined as

$$\begin{aligned} &\mathbf{P}(\mathbf{D}_{i+1}^n, \mathbf{R}^n) \approx \mathbf{P}(\mathbf{D}_i^n, \mathbf{R}^n) + \frac{\partial \mathbf{P}(\mathbf{D}_i^n, \mathbf{R}^n)}{\partial \mathbf{D}} \delta\mathbf{D}_i^n = \mathbf{0} \\ \text{where} \quad &\mathbf{D}_{i+1}^n = \mathbf{D}_i^n + \delta\mathbf{D}_i^n \end{aligned} \tag{2.9}$$

Here i defines the iteration number for load step n. The configuration at iteration i is given by the displacements $\mathbf{D}_i^n$ and load $\mathbf{R}^n$. Furthermore, the tangent stiffness matrix is defined as $\dfrac{\partial \mathbf{P}(\mathbf{D}_i^n, \mathbf{R}^n)}{\partial \mathbf{D}} = \dfrac{\partial \mathbf{F}(\mathbf{D}_i^n)}{\partial \mathbf{D}} \equiv \mathbf{K}_T(\mathbf{D}_i^n)$. Additionally, proportional loads are assumed meaning $\mathbf{R}^n = \overline{\mathbf{R}}\gamma^n$ where γ^n is the scaling of the reference load vector $\overline{\mathbf{R}}$. If the above considerations are inserted into Eq. (2.9) the nonlinear incremental equilibrium equations are obtained.

$$\begin{aligned} &\mathbf{K}_T\left(\mathbf{D}_i^n\right) \delta\mathbf{D}_i^n = \overline{\mathbf{R}}\gamma^n - \mathbf{F}^n\left(\mathbf{D}_i^n\right) \\ \text{where} \quad &\mathbf{K}_T\left(\mathbf{D}_i^n\right) = \mathbf{K}_0 + \mathbf{K}_L\left(\mathbf{D}_i^n\right) + \mathbf{K}_S\left(\mathbf{D}_i^n\right) \\ \text{or} \quad &\mathbf{K}_T^n = \mathbf{K}_0 + \mathbf{K}_L^n + \mathbf{K}_S^n \end{aligned} \tag{2.10}$$

Here $\mathbf{K}_L$ is the displacement stiffness matrix and $\mathbf{K}_S$ the stress stiffness matrix. At a converged load step the parenthesis may be omitted for simplicity, thus $\mathbf{K}_T\left(\mathbf{D}^n\right) \equiv \mathbf{K}_T^n$. In the above formulation the displacements refer to the initial (undeformed) configuration, which is called the Total Lagrangian Form, see e.g., [28].

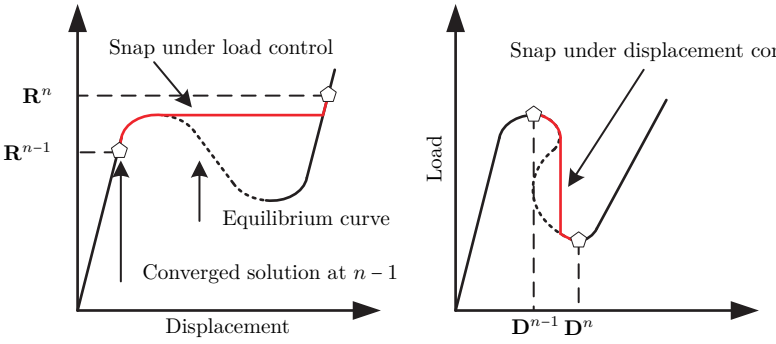

Figure 2.2: Sketch of snap through and snap back. Snap through is shown in the left figure and can be encountered for a nonlinear solver under load control. Here an increase in load above the load limit point results in finite displacements. Snap back is when the response curve "turns back" in itself with the appearance of a turning point (displacement limit point). Both of these snapping phenomenons may result in convergence issues for the solvers.

Traditional Newton iterative solvers can be used to solve these equations, but as the analysis will be performed in the vicinity of critical points, the arc-length solver from [29, 30] is used, as the Newton solvers are unable to traverse general critical points. This can be seen by considering a limit point instability shown in e.g., Figure 2.2. Standard Newton solvers may sometimes fail to converge in the case of limit point instabilities, and upon convergence it will snap and not trace the part of the equilibrium curve under the red line.

2.4.2 Linear buckling analysis

If the pre-buckling response is linear the displacement stiffness matrix $\mathbf{K}_L = \mathbf{0}$, and the tangent stiffness matrix is approximated using only the linear stiffness and stress stiffness matrices $\mathbf{K}_0$ and $\mathbf{K}_S$, respectively. The stress stiffness matrix is formulated based on the stresses from a linear static analysis, Eq. (2.4), and it is assumed to scale linearly with the load. Consequently, Eq. (2.7) is reduced to

$$(\mathbf{K}_0 + \lambda_j \mathbf{K}_S)\,\boldsymbol{\phi}_j = \mathbf{0}, \quad j = 1, 2, \ldots \tag{2.11}$$

The eigenvalues, λ_j, are assumed being ordered in magnitude such that λ_1 is the lowest. Linear buckling analysis only determines bifurcation buckling, as limit point buckling is caused by nonlinearities of the fundamental equilibrium curve. Furthermore, the analyst cannot know a priori whether linear buckling analysis is adequate to capture the buckling response of a structure, thus linear buckling analysis should be used with care.

2.4.3 Nonlinear buckling analysis

In the linear buckling analysis, it is assumed that the pre-buckling displacements are small, so they do not influence the response of the structure. If the pre-buckling displacements cannot be ignored, the full tangent stiffness matrix from Eq. (2.10) must be utilized. The nonlinear buckling analysis applied in this work is based on the contributions in [31–36], and the approach is described in the following.

To perform a nonlinear buckling analysis, a geometrically nonlinear analysis is performed, and during the analysis the load factor, γ, is monitored. The GNL buckling analysis can capture both bifurcation and limit point instabilities. A limit point is detected when the load factor decreases between two equilibrium points. Tangent stiffness information is used to detect a bifurcation point. At the critical point, the tangent stiffness matrix is singular, hence Eq. (2.7) is satisfied, and if the load does not decrease in the following equilibrium points, a bifurcation point is detected. To avoid an exact determination of the critical point, the so-called one point approach is used [28]. Additionally, this method gives information concerning an upcoming critical point and whether a critical point has been passed. This approach uses the tangent stiffness matrix information at the current load step to estimate the critical point. It is assumed that the difference between the current configuration, n, and the critical configuration, c, is small such that the displacements do not change, meaning that $\mathbf{K}_L^n \approx \mathbf{K}_L^c$. Furthermore, the stress stiffness matrix is assumed to scale linearly with the load to the critical point $\mathbf{K}_S^c \approx \lambda \mathbf{K}_S^n$, see also [34]. This is inserted into Eq. (2.7) hereby obtaining

$$\left(\mathbf{K}_0 + \mathbf{K}_L^n + \lambda_j \mathbf{K}_S^n\right) \boldsymbol{\phi}_j = \mathbf{0} \tag{2.12}$$

From the nonlinear stability equation the scaling between the current and critical load factor can be obtained as

$$\gamma_j^c = \lambda_j \gamma^n \tag{2.13}$$

From this it is seen that $\lambda_1 > 1$ means that a critical point is upcoming, whereas $\lambda_1 < 1$ means that a critical point has been passed. This approach has been shown to converge in the limit of the critical load [28]. Nonlinear buckling analysis is more accurate than linear buckling analysis, with the expense that the analysis needed to determine the critical point becomes nonlinear, and thus an iterative method is needed to trace the equilibrium curve, making it computationally expensive compared to linear buckling analysis.

2.5 Buckling optimization

When performing buckling optimization the primary interest is to maximize or constrain the buckling load factors, λ_j for the linear problem and γ_j^c for the nonlinear problem, hereby securing that buckling does not occur during operation. Buckling optimization typically does not consider the post-buckling

response of a structure, which is altered during the optimization process. The design sensitivities in this work are determined by the direct differentiation method. In this approach the governing equations are differentiated with respect to a design variable a_i to obtain the sensitivities. This is combined with semi-analytical design sensitivity analysis where the derivatives of the stiffness matrices are approximated by central differences at the element level. Using semi-analytical design sensitivity analysis allows for easy implementation of different parametrizations like fiber angles, DMO, thickness etc. In the case of linear buckling analysis, Eq. (2.11) is differentiated, pre-multiplied by $\boldsymbol{\phi}_j^T$, and $\frac{\mathrm{d}\lambda_j}{\mathrm{d}a_i}$ is isolated

$$\frac{\mathrm{d}\lambda_j}{\mathrm{d}a_i} = \boldsymbol{\phi}_j^T \left(\frac{\mathrm{d}\mathbf{K}_0}{\mathrm{d}a_i} + \lambda_j \frac{\mathrm{d}\mathbf{K}_S}{\mathrm{d}a_i} \right) \boldsymbol{\phi}_j \tag{2.14}$$

In the derivation it is used that $\mathbf{K}_0$ and $\mathbf{K}_S$ are symmetric, and that the eigenvectors are orthonormalized such that $\boldsymbol{\phi}_j^T \left(-\mathbf{K}_S\right) \boldsymbol{\phi}_j = 1$. In the equation above it is important to note that the linear stiffness matrix, $\mathbf{K}_0$, is only a function of the design variables associated with the element, whereas $\frac{\mathrm{d}\mathbf{K}_S}{\mathrm{d}a_i}$ is a function of the displacements, hence is dependent on all elements. The displacement sensitivities are obtained by differentiating Eq. (2.4)

$$\mathbf{K}_0 \frac{\mathrm{d}\mathbf{D}}{\mathrm{d}a_i} = -\frac{\mathrm{d}\mathbf{K}_0}{\mathrm{d}a_i}\mathbf{D} + \underbrace{\frac{\mathrm{d}\mathbf{R}}{\mathrm{d}a_i}}_{=\mathbf{0}} \tag{2.15}$$

From this it is possible to determine the sensitivities of $\mathbf{K}_0$ and $\mathbf{K}_S$ using central differences at the element level

$$\begin{aligned}
\frac{\mathrm{d}\mathbf{K}_0^e}{\mathrm{d}a_i} &= \frac{\mathbf{K}_0^e\left(a_i + \Delta a_i\right) - \mathbf{K}_0^e\left(a_i - \Delta a_i\right)}{2\Delta a_i} \\
\frac{\mathrm{d}\mathbf{K}_S^e}{\mathrm{d}a_i} &= \frac{\mathbf{K}_S^e\left(a_i + \Delta a_i, \mathbf{D}^e + \Delta\mathbf{D}^e\right) - \mathbf{K}_S^e\left(a_i - \Delta a_i, \mathbf{D}^e - \Delta\mathbf{D}^e\right)}{2\Delta a_i} \\
&\text{where } \Delta\mathbf{D}^e \approx \frac{\mathrm{d}\mathbf{D}^e}{\mathrm{d}a_i}\Delta a_i
\end{aligned}$$

Here a superscript ^{e} defines an element quantity.

Next design sensitivity analysis for the nonlinear buckling analysis is considered. The approach is based on [31–33]. This approach is much similar to the linear buckling design sensitivity analysis. Differentiating and rearranging Eq. (2.12) in a similar manner as for the linear buckling design sensitivity analysis, the sensitivities of the eigenvalues for the GNL buckling analysis are obtained

$$\frac{\mathrm{d}\lambda_j}{\mathrm{d}a_i} = \boldsymbol{\phi}_j^T \left(\frac{\mathrm{d}\mathbf{K}_0}{\mathrm{d}a_i} + \frac{\mathrm{d}\mathbf{K}_L^n}{\mathrm{d}a_i} + \lambda_j \frac{\mathrm{d}\mathbf{K}_S^n}{\mathrm{d}a_i} \right) \boldsymbol{\phi}_j \tag{2.16}$$

Here the sensitivities of the stiffness matrices are calculated in the same manner as in the linear design sensitivity analysis. To obtain the displacement

sensitivities the nonlinear equilibrium equations are differentiated

$$\begin{aligned} &\frac{\mathrm{d}\mathbf{P}}{\mathrm{d}a_i} = \frac{\partial \mathbf{P}}{\partial a_i} + \frac{\partial \mathbf{P}}{\partial \mathbf{D}^n}\frac{\mathrm{d}\mathbf{D}^n}{\mathrm{d}a_i} = \mathbf{0} \\ &\Updownarrow \\ &\mathbf{K}_T^n \frac{\mathrm{d}\mathbf{D}^n}{\mathrm{d}a_i} + \frac{\partial \mathbf{F}}{\partial a_i} - \underbrace{\frac{\mathrm{d}\mathbf{R}}{\mathrm{d}a_i}}_{=\mathbf{0}} = \mathbf{0} \end{aligned} \tag{2.17}$$

Recall that $\mathbf{K}_T^n \equiv \dfrac{\partial \mathbf{P}}{\partial \mathbf{D}^n}$. From this, the sensitivities of the buckling load factor, γ, is determined by differentiating Eq. (2.13).

$$\frac{\mathrm{d}\gamma_j^c}{\mathrm{d}a_i} = \frac{\mathrm{d}\lambda_j}{\mathrm{d}a_i}\gamma^n \tag{2.18}$$

2.5.1 Imperfection sensitivity optimization

When optimizing the buckling load factor, the optimized structure is often claimed to be more sensitive towards imperfections [37]. Consequently, robust buckling design optimization procedures which take imperfections into account during the optimization should be applied. One approach is to apply probabilistic methods in the design process, where the imperfections are quantified with respect to mean value and standard deviation, see e.g., [38] for a review. In this approach the effects of various imperfections are determined, and structures which are optimal towards the most common imperfections can be designed. A large database is required to have sufficient imperfection data to perform such optimization for the specific structure of interest. An other design concept is to perform worst case optimization, where the performance of the structure including the worst imperfections is optimized. This concept may be applied in the initial design phase where little information concerning "the real" imperfections is present.

In this work the concept of "worst" shape imperfection is applied. Here all imperfections are represented by an equivalent geometric imperfection. To impose the imperfection a number of base shapes are defined. The base shapes are e.g., buckling mode shapes, imperfection measurements etc., see also Figure 2.3. In the "worst" shape imperfection optimization the linear combination of the base shapes which minimizes the buckling load is determined

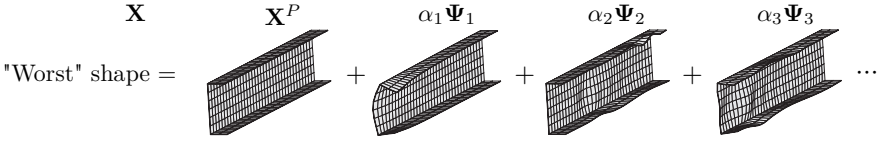

Figure 2.3: Representation of the "worst" shape imperfection by perturbation of the perfect structure, $\mathbf{X}^P$, by a set of base shapes, $\alpha_k \boldsymbol{\Psi}_k$.

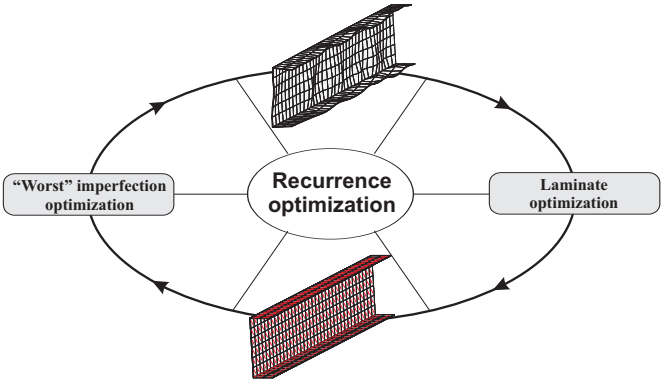

Figure 2.4: Schematic representation of the recurrence optimization.

[32, 39–42]. Combining this with a laminate optimization used to maximize the buckling load for the imperfect structure results in the recurrence optimization from [32]. The recurrence optimization is shown in Figure 2.4, and either of two optimizations is performed in a sequential manner:

1. For a given laminate layup; determine the geometric imperfection which minimizes the nonlinear buckling load, or

2. For an imperfect structure; determine the laminate layup which maximizes the nonlinear buckling load.

By continuously switching between the two optimizations the buckling load of the "worst" shape imperfect structure is maximized. A recurrence optimization process is given in Figure 2.5. During the recurrence optimization the buckling load for the imperfect structure is increased. The result is that the buckling load of the "worst" structure is maximized. The cost is that the buckling load for the idealized perfect structure is decreased. This decrease can be evaluated by analyzing the structure without any imperfections. The difference between the buckling load of the perfect structure and the buckling load of the structure with the "worst" shape imperfection imposed represents a measure of the imperfection sensitivity of the structure. A small difference between the perfect and imperfect structure represents a structure with a low imperfection sensitivity and vise versa.

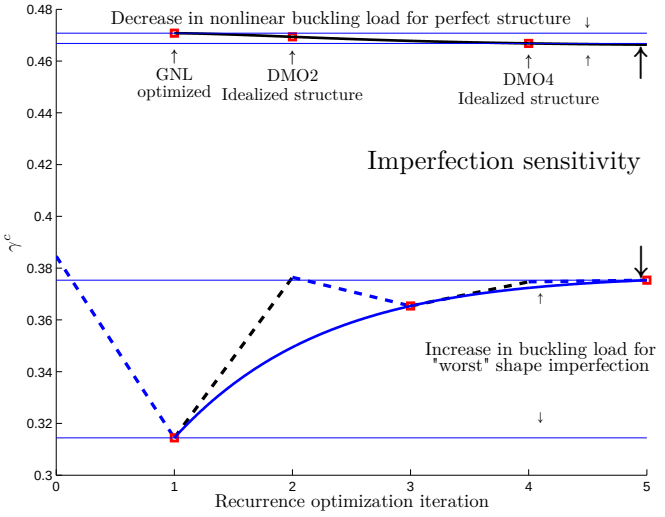

Figure 2.5: Recurrence optimization of a structure. The dashed lines are the results from the recurrence optimization. The top red boxes are the laminate designs evaluated on the perfect structure. The imperfection sensitivity is defined as the difference between the idealized buckling load and the imperfect buckling load.

2.6 Asymptotic post-buckling analysis

Post-buckling analysis is used to determine the response of a structure after a critical point has been passed. The analysis provides information concerning the post-buckling deformations and whether the post-buckling response is stable or unstable. Furthermore, post-buckling stability is closely related to the imperfection sensitivity of the structure, see also Figure 1.9-1.11.

To perform a post-buckling analysis on the full finite element model, an approach similar to geometrically nonlinear finite element analysis described in section 2.4 is required. Since the post-buckling response may become unstable, a solver like the arc-length solver has desirable properties as it is able to trace unstable equilibrium curves. If a bifurcation point is present the solver may not switch branch and follow the unstable fundamental equilibrium curve. One method to force branch switching is to apply an imperfection, which has been demonstrated in section 1.3. The multiple equilibrium curves are replaced by a single equilibrium curve and branching is automatically performed. GNL analysis can be difficult and time consuming when having several load cases and a complex structural response. One method to reduce the complexity and extract the most important properties of the post-buckling response is to use asymptotic methods. Asymptotic methods substitute the full and complex response by a series of simpler problems [43]. Much research within asymptotic post-buckling analysis is based on the work by Koiter [44], see also [45, 46] for

an exhaustive description of the analytical approach to Koiter analysis. The analysis method has been extended to multiple buckling loads and nonlinear pre-buckling in [47, 48], respectively. Koiter analysis has been implemented within a finite element framework where shell and beam elements have been used [49–53], and using the differential quadrature method in [54]. In the standard Koiter analysis only the first two terms in the expansions are of interest as these describe the stability in the vicinity of the critical point and the type of stability. If the response further in the post-buckling regime is required more terms are needed in the expansion. In such case Padé approximants has proven to be more effective than the Taylor-like expansion from Koiter analysis [55, 56].

The primary interest is in the initial response, thus Koiter's method is considered in this work. Assuming that the load and deformation for the critical point ^{c} are known, the initial post-buckling response is represented by a Taylor-like expansion, where the expanded load factor, λ, displacements, $\boldsymbol{u}$, strains, $\boldsymbol{\epsilon}$, and stresses, $\boldsymbol{\sigma}$, are extrapolated into the post-buckling regime as

$$\lambda = \lambda_c + a\lambda_c\xi + b\lambda_c\xi^2 + c\lambda_c\xi^3 + \dots \tag{2.19}$$

$$\begin{aligned}\boldsymbol{u} &= \lambda^0\boldsymbol{u} + {}^1\boldsymbol{u}\xi + \tilde{\boldsymbol{u}} \\ &= \lambda^0\boldsymbol{u} + {}^1\boldsymbol{u}\xi + \sum_{j=2}^{\infty} {}^j\boldsymbol{u}\xi^j\end{aligned} \tag{2.20}$$

$$\boldsymbol{\epsilon} = \lambda^0\boldsymbol{\epsilon} + {}^1\boldsymbol{\epsilon}\xi + {}^2\boldsymbol{\epsilon}\xi^2 + {}^3\boldsymbol{\epsilon}\xi^3 + \dots \tag{2.21}$$

$$\boldsymbol{\sigma} = \lambda^0\boldsymbol{\sigma} + {}^1\boldsymbol{\sigma}\xi + {}^2\boldsymbol{\sigma}\xi^2 + {}^3\boldsymbol{\sigma}\xi^3 + \dots \tag{2.22}$$

Here a superscript ^{0} defines a pre-buckling quantity, whereas all higher quantities are related to the post-buckling state. a, b, and c are the linear, quadratic, and cubic Koiter-factors. A geometric interpretation of the a and b-factors is given in Figure 2.6. The a-factor is the slope of the initial post-buckling response and the b-factor is the curvature. Through the derivation the terms are grouped by the powers of the perturbation parameter, ξ, and for $\xi \to 0$ the structure approaches the critical configuration. Considering the expanded displacement field, $\boldsymbol{u}$, the expansion from the critical pre-buckling configuration ${\lambda_c}^0\boldsymbol{u}$ to the post-buckled configuration $\boldsymbol{u}$ is stipulated to follow ${}^1\boldsymbol{u}$ and a correction term $\tilde{\boldsymbol{u}}$ which is formed based on the higher order buckling mode shapes ${}^2\boldsymbol{u}$, ${}^3\boldsymbol{u}$, etc. Some important aspects should be noted about the expansions:

1. The post-buckling quantities: a, b, ${}^p\boldsymbol{u}$, ${}^p\boldsymbol{\epsilon}$, and ${}^p\boldsymbol{\sigma}$, $p \geq 1$, are decoupled from the pre-buckling response[1].

2. The ${}^2\boldsymbol{u}$, ${}^3\boldsymbol{u}$, … displacement fields are used to correct the predicted post-buckling field from ${}^1\boldsymbol{u}$. Accordingly, they are given the following orthogonality properties: ${}^1\boldsymbol{\sigma} \cdot l_1\left({}^q\boldsymbol{u}\right) = {}^0\boldsymbol{\sigma} \cdot l_{11}\left({}^1\boldsymbol{u}, {}^q\boldsymbol{u}\right) = 0$, $q \geq 2$. This is

[1] In the remainder of the section, when a superscript ^{p} is used in front of a (Greek) letter it defines a post-buckling field: ${}^1\boldsymbol{u}, {}^1\boldsymbol{\epsilon}, {}^1\boldsymbol{\sigma}, {}^2\boldsymbol{u}, {}^2\boldsymbol{\epsilon}, {}^2\boldsymbol{\sigma}$ etc.

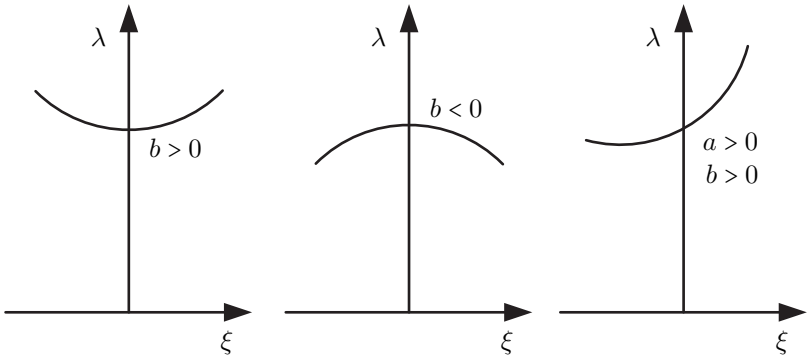

Figure 2.6: Definition of the Koiter a and b-factors. The plots display the perturbation of the load factor λ in the post-buckling regime. a and b represent the slope and the curvature of the post-buckling response, respectively. $a = 0$ in the left and center figures. The only stable response is the one in the left figure. When $a \neq 0$ the response is always unstable regardless of the sign of a, but for $b > 0$ stability is recovered in the post-buckling regime.

equivalent to ${}^1\mathbf{U}^T\mathbf{K}_0{}^q\mathbf{U} = {}^1\mathbf{U}^T\mathbf{K}_S{}^q\mathbf{U} = 0$ on finite element form. ${}^2\boldsymbol{u}$, ${}^3\boldsymbol{u}$, ..., are not given any mutual orthogonality properties.

3. The stability of the structure is determined by the Koiter a and b-factors, where only one combination can give an initial stable post-buckling response: $a = 0$ and $b > 0$, see Figure 2.6[2]. $a \neq 0$ and $b > 0$ gives a structural response which initially is unstable, but it recovers the stability.

4. For $\xi = 0$ the structure is in the critical configuration.

5. The expansion cannot handle phenomena like mode switching, secondary instabilities etc., as only the responses included into the expansion can be accounted for.

The equations needed in the Koiter analysis are derived using the Budiansky-Hutchinson notation due to the simplicity of the equations compared to using index notation. In the Budiansky-Hutchinson notation the strain is given by the following definition

$$\boldsymbol{\epsilon} = l_1(\boldsymbol{u}) + \frac{1}{2} l_2(\boldsymbol{u}) \tag{2.23}$$

The strain consists of a linear homogenous operator, l_1, and a quadratic homogenous operator, l_2. The properties of the operators vary with respect to the applied theory i.e., beam, plate, shell etc. Here the focus is on the continuum version, and to obtain a description of the operators they are compared

[2]Note that in a numerical framework $a \equiv 0$ is nearly impossible to obtain, and thus $a = 0$ should be interpreted as $|a| \ll b$.

to tensor notation

$$\epsilon_{ij} = \underbrace{\frac{1}{2}\left(u_{i,j} + u_{j,i}\right)}_{l_1(\boldsymbol{u})} + \underbrace{\frac{1}{2}\left(u_{k,i}u_{k,j}\right)}_{l_2(\boldsymbol{u})} \tag{2.24}$$

From this a definition of the operators is obtained. If Eq. (2.20), (2.21), (2.23), and (2.24) are considered, the link between the expanded displacements and strains can be established. Inserting the expanded displacements, Eq. (2.20), into the strain definition, Eq. (2.24), the expanded strains on tensor notation are given as

$$\begin{aligned}\epsilon_{ij} =& \frac{1}{2}\left(\lambda^0 u_{i,j} + \lambda^0 u_{j,i} + \left(\lambda^2\right){}^0u_{k,i}{}^0u_{k,j}\right) + \frac{1}{2}\left({}^1u_{i,j} + {}^1u_{j,i} + {}^1u_{k,i}{}^1u_{k,j}\xi\right)\xi \\ &+ \frac{1}{2}\left({}^2u_{i,j} + {}^2u_{j,i} + {}^2u_{k,i}{}^2u_{k,j}\xi^2\right)\xi^2 + \frac{1}{2}\left({}^3u_{i,j} + {}^3u_{j,i} + {}^3u_{k,i}{}^3u_{k,j}\xi^3\right)\xi^3 \\ &+ \frac{1}{2}\left(\lambda^0 u_{k,i}{}^1u_{k,j} + \lambda^0 u_{k,j}{}^1u_{k,i}\right)\xi + \frac{1}{2}\left(\lambda^0 u_{k,i}{}^2u_{k,j} + \lambda^0 u_{k,j}{}^2u_{k,i}\right)\xi^2 \\ &+ \frac{1}{2}\left(\lambda^0 u_{k,i}{}^3u_{k,j} + \lambda^0 u_{k,j}{}^3u_{k,i} + {}^1u_{k,i}{}^2u_{k,j} + {}^1u_{k,j}{}^2u_{k,i}\right)\xi^3 + \ldots\end{aligned} \tag{2.25}$$

Recall that a linear pre-buckling response is assumed, thus the quadratic term ${}^0u_{k,i}{}^0u_{k,j}$ vanish. Furthermore, the derivatives of ${}^0u$ are small, thus any product involving the pre-buckling quantity is at least one order of magnitude smaller than the other terms, hence can be removed. This reduces Eq. (2.25) to

$$\begin{aligned}\epsilon_{ij} =& \frac{1}{2}\lambda\left({}^0u_{i,j} + {}^0u_{j,i}\right) + \frac{1}{2}\left({}^1u_{i,j} + {}^1u_{j,i}\right)\xi + \frac{1}{2}\left({}^2u_{i,j} + {}^2u_{j,i} + {}^1u_{k,i}{}^1u_{k,j} +\right)\xi^2 \\ &+ \frac{1}{2}\left({}^3u_{i,j} + {}^3u_{j,i} + {}^1u_{k,i}{}^2u_{k,j} + {}^1u_{k,j}{}^2u_{k,i}\right)\xi^3 + \ldots\end{aligned} \tag{2.26}$$

In the expansion of the quadratic term in the strain definition, a bilinear term is obtained. This is represented by the symmetric l_{11} operator in the Budiansky-Hutchinson notation and has the following properties

$$\begin{aligned} l_2(\boldsymbol{u}+\boldsymbol{v}) &= l_2(\boldsymbol{u}) + 2l_{11}(\boldsymbol{u},\boldsymbol{v}) + l_2(\boldsymbol{v}) \\ l_{11}(\boldsymbol{u},\boldsymbol{v}) &= \frac{1}{2}\left(u_{k,i}v_{k,j} + u_{k,j}v_{k,i}\right)\end{aligned} \tag{2.27}$$

Furthermore, the l operators possess the following properties

$$\begin{aligned} &l_1(k\boldsymbol{u}) = kl_1(\boldsymbol{u}), && l_1(\boldsymbol{u}+\boldsymbol{v}) = l_1(\boldsymbol{u}) + l_1(\boldsymbol{v}) \\ &l_2(k\boldsymbol{u}) = k^2 l_2(\boldsymbol{u}), && l_{11}(k_1\boldsymbol{u}, k_2\boldsymbol{v}) = k_1k_2l_{11}(\boldsymbol{u},\boldsymbol{v}) \\ &l_{11}(\boldsymbol{u},\boldsymbol{u}) = l_2(\boldsymbol{u}) && \end{aligned} \tag{2.28}$$

From Eq. (2.26) the expanded strains are given in the Budiansky-Hutchinson notation as

$$\boldsymbol{\epsilon} = \underbrace{\lambda l_1\left({}^0\boldsymbol{u}\right)}_{{}^0\boldsymbol{\epsilon}} + \underbrace{l_1\left({}^1\boldsymbol{u}\right)}_{{}^1\boldsymbol{\epsilon}}\xi + \underbrace{\left(l_1\left({}^2\boldsymbol{u}\right) + \frac{1}{2}l_2\left({}^1\boldsymbol{u}\right)\right)}_{{}^2\boldsymbol{\epsilon}}\xi^2 + \underbrace{\left(l_1\left({}^3\boldsymbol{u}\right) + l_{11}\left({}^1\boldsymbol{u}, {}^2\boldsymbol{u}\right)\right)}_{{}^3\boldsymbol{\epsilon}}\xi^3 + \ldots \tag{2.29}$$

By comparing Eq. (2.25), (2.26), and (2.29), it is observed that $l_2\left({}^0\boldsymbol{u}\right) = l_{11}\left({}^0\boldsymbol{u}, \boldsymbol{v}\right) = 0$. This follows from the discussion that the derivatives of ${}^0\boldsymbol{u}$ are small. The post-buckling displacement fields, ${}^p\boldsymbol{u}$, are nonlinear, and thus the nonlinear part of the strain definition from Eq. (2.27) cannot be neglected. The strain fields are defined based on the powers of ξ and not a displacement field i.e., $\boldsymbol{\epsilon}\left({}^1\boldsymbol{u}\right) \neq {}^1\boldsymbol{\epsilon}$. The stresses are defined based on the expanded strains. Assuming linear elasticity the stresses are given through the linear homogeneous constitutive H-operator

$$\boldsymbol{\sigma} = H\left(\boldsymbol{\epsilon}\right) \tag{2.30}$$

The equivalent tensor form with $H = C_{ijkl}$ is

$$\sigma_{ij} = C_{ijkl}\epsilon_{kl}$$

The principle of virtual displacements is used to derive the equations for the asymptotic analysis. In tensor form the variational form of the total elastic potential is given by [45, 57]

$$\begin{aligned}\delta\Pi(u_i) &= \int_V \sigma_{ij}\delta\epsilon_{ij}\ \mathrm{d}V - \int_V \lambda\overline{B}_i\delta u_i\ \mathrm{d}V - \int_S \lambda\overline{F}_i\delta u_i\ \mathrm{d}S - \sum_{k=1}^{n^k} \lambda\overline{R}_i^k\delta u_i^k \\ &= \int_V \sigma_{ij}\delta\epsilon_{ij}\ \mathrm{d}V - \int_\Omega \lambda\overline{T}_i\delta u_i\ \mathrm{d}\Omega = 0\end{aligned} \tag{2.31}$$

Here $\overline{B}_i$, $\overline{F}_i$, and $\overline{R}_i$ are the load distributions for body, surface, and point loads, respectively, and they are collected in $\overline{T}_i$, where Ω defines definite integration. Proportional loading is assumed, thus λ is the scaling of the reference loads. Using the Budiansky-Hutchinson notation the variation of the total potential energy is given by

$$\delta\Pi(\boldsymbol{u}) = \boldsymbol{\sigma}\cdot\delta\boldsymbol{\epsilon} - \lambda\overline{\boldsymbol{T}}\cdot\delta\boldsymbol{u} = 0 \tag{2.32}$$

The $\cdot$ operator defines a multiplication and definite integration. The total variation of the strains is given by

$$\begin{aligned}\delta^{(T)}\boldsymbol{\epsilon} &= \boldsymbol{\epsilon}\left(\boldsymbol{u} + \delta\boldsymbol{u}\right) - \boldsymbol{\epsilon}\left(\boldsymbol{u}\right) \\ &= l_1\left(\boldsymbol{u}\right) + l_1\left(\delta\boldsymbol{u}\right) + \frac{1}{2}l_2\left(\boldsymbol{u}\right) + l_{11}\left(\boldsymbol{u}, \delta\boldsymbol{u}\right) + \frac{1}{2}l_2\left(\delta\boldsymbol{u}\right) - l_1\left(\boldsymbol{u}\right) - \frac{1}{2}l_2\left(\boldsymbol{u}\right) \\ &= l_1\left(\delta\boldsymbol{u}\right) + l_{11}\left(\boldsymbol{u}, \delta\boldsymbol{u}\right) + l_2\left(\delta\boldsymbol{u}\right)\end{aligned} \tag{2.33}$$

The first variation can be represented by Eq. (2.34), as $l_2\left(\delta\boldsymbol{u}\right)$ is of higher order.

$$\delta^{(1)}\boldsymbol{\epsilon} \equiv \delta\boldsymbol{\epsilon} = l_1\left(\delta\boldsymbol{u}\right) + l_{11}\left(\boldsymbol{u}, \delta\boldsymbol{u}\right) \tag{2.34}$$

The next step is to insert the expansions into Eq. (2.32) and collect these in the powers of ξ

$$
\begin{aligned}
&\underbrace{{\lambda_c}^0\boldsymbol{\sigma}\cdot l_1(\delta\boldsymbol{u}) - \lambda_c\overline{\boldsymbol{T}}\cdot\delta\boldsymbol{u}}_{\text{Zeroth order problem}} \\
&+\underbrace{\left[{\lambda_c}^0\boldsymbol{\sigma}\cdot l_{11}\left({}^1\boldsymbol{u},\delta\boldsymbol{u}\right) + {}^1\boldsymbol{\sigma}\cdot l_1(\delta\boldsymbol{u}) + a\lambda_c\left({}^0\boldsymbol{\sigma}\cdot l_1(\delta\boldsymbol{u}) - \overline{\boldsymbol{T}}\cdot\delta\boldsymbol{u}\right)\right]}_{\text{First order problem}}\xi \\
&+\underbrace{\left[{\lambda_c}^0\boldsymbol{\sigma}\cdot l_{11}\left({}^2\boldsymbol{u},\delta\boldsymbol{u}\right) + \left(a{\lambda_c}^0\boldsymbol{\sigma} + {}^1\boldsymbol{\sigma}\right)\cdot l_{11}\left({}^1\boldsymbol{u},\delta\boldsymbol{u}\right) + {}^2\boldsymbol{\sigma}\cdot l_1(\delta\boldsymbol{u})\right]}_{\text{Second order problem}}\xi^2 \\
&+\quad\underbrace{b\lambda_c\left({}^0\boldsymbol{\sigma}\cdot l_1(\delta\boldsymbol{u}) - \overline{\boldsymbol{T}}\cdot\delta\boldsymbol{u}\right)}_{\text{Second order problem cont'd}}\quad\xi^2 \\
&+\underbrace{\left[{\lambda_c}^0\boldsymbol{\sigma}\cdot l_{11}\left({}^3\boldsymbol{u},\delta\boldsymbol{u}\right) + {}^3\boldsymbol{\sigma}\cdot l_1(\delta\boldsymbol{u}) + \left(a{\lambda_c}^0\boldsymbol{\sigma} + {}^1\boldsymbol{\sigma}_1\right)\cdot l_{11}\left({}^2\boldsymbol{u},\delta\boldsymbol{u}\right)\right]}_{\text{Third order problem}}\xi^3 \\
&+\underbrace{\left[\left(b{\lambda_c}^0\boldsymbol{\sigma} + {}^2\boldsymbol{\sigma}\right)\cdot l_{11}\left({}^1\boldsymbol{u},\delta\boldsymbol{u}\right) + c\lambda_c\left({}^0\boldsymbol{\sigma}\cdot l_1(\delta\boldsymbol{u}) - \overline{\boldsymbol{T}}\cdot\delta\boldsymbol{u}\right)\right]}_{\text{Third order problem cont'd}}\xi^3 + \cdots = 0
\end{aligned}
\tag{2.35}
$$

This equation must be valid for any value of ξ, and thus each coefficient in the expansion must be zero. If Eq. (2.35) is considered, some important aspects can be deduced. The GNL equilibrium equations in Eq. (2.10) are replaced by a series of simpler linear problems. Furthermore, the zeroth order problem relies on pre-buckling information i.e., ${}^0\boldsymbol{u}$ and ${}^0\boldsymbol{\sigma}$, the first order problem only on the zeroth and first order information i.e., ${}^0\boldsymbol{u}$, ${}^1\boldsymbol{u}$, ${}^0\boldsymbol{\epsilon}$, ${}^1\boldsymbol{\epsilon}$, ${}^0\boldsymbol{\sigma}$, ${}^1\boldsymbol{\sigma}$, a etc., therefore, the problem can be solved sequentially. Consequently, if a higher precision is required in the expansion more terms can be included. As only the initial post-buckling response is of interest in this work, the problems up to the third order are considered. Based on Eq. (2.35) the equations to obtain ${}^0\boldsymbol{u}$, ${}^1\boldsymbol{u}$, ${}^2\boldsymbol{u}$, a, b, and λ_c can be established. The zeroth order problem is the linear equilibrium equations, and the problem is used to determine ${}^0\boldsymbol{u}$ by

$${}^0\boldsymbol{\sigma}\cdot l_1(\delta\boldsymbol{u}) - \overline{\boldsymbol{T}}\cdot\delta\boldsymbol{u} = 0 \tag{2.36}$$

It is important to note that this equation is present in all terms, thus the expansion for the higher order terms in Eq. (2.35) is reduced to

$$
\begin{aligned}
&\left[{\lambda_c}^0\boldsymbol{\sigma}\cdot l_{11}\left({}^1\boldsymbol{u},\delta\boldsymbol{u}\right) + {}^1\boldsymbol{\sigma}\cdot l_1(\delta\boldsymbol{u})\right]\xi \\
&+\left[{\lambda_c}^0\boldsymbol{\sigma}\cdot l_{11}\left({}^2\boldsymbol{u},\delta\boldsymbol{u}\right) + \left(a{\lambda_c}^0\boldsymbol{\sigma} + {}^1\boldsymbol{\sigma}\right)\cdot l_{11}\left({}^1\boldsymbol{u},\delta\boldsymbol{u}\right) + {}^2\boldsymbol{\sigma}\cdot l_1(\delta\boldsymbol{u})\right]\xi^2 \\
&+\left[{\lambda_c}^0\boldsymbol{\sigma}\cdot l_{11}\left({}^3\boldsymbol{u},\delta\boldsymbol{u}\right) + {}^3\boldsymbol{\sigma}\cdot l_1(\delta\boldsymbol{u}) + \left(a{\lambda_c}^0\boldsymbol{\sigma} + {}^1\boldsymbol{\sigma}_1\right)\cdot l_{11}\left({}^2\boldsymbol{u},\delta\boldsymbol{u}\right)\right]\xi^3 \\
&+\left[\left(b{\lambda_c}^0\boldsymbol{\sigma} + {}^2\boldsymbol{\sigma}\right)\cdot l_{11}\left({}^1\boldsymbol{u},\delta\boldsymbol{u}\right)\right]\xi^3 + \cdots = 0
\end{aligned}
$$

From this reduction it follows that the a-factor is eliminated from the first order problem, the b-factor from the second order problem etc. Consequently, the sec-

ond order problem is required to determine the a-factor, the third order problem to determine the b-factor and so on. To determine the j'th post-buckling displacement field the j'th order problem is needed i.e., ${}^1\boldsymbol{u}$ is determined from the first order problem. The first order problem is the linear buckling problem, which is used to determine ${}^1\boldsymbol{u}$ and λ_c

$$ {}^1\boldsymbol{\sigma} \cdot l_1\left(\delta\boldsymbol{u}\right) + \lambda_c{}^0\boldsymbol{\sigma} \cdot l_{11}\left({}^1\boldsymbol{u}, \delta\boldsymbol{u}\right) = 0 \tag{2.37} $$

The link between Eq. (2.11) and Eq. (2.37) might be difficult to see, but it can be established using Table 2.1. To determine the second post-buckling displacement field, ${}^2\boldsymbol{u}$, and the Koiter a-factor, one may assume without loss of generality that the variation of the displacement field has the form

$$ \delta\boldsymbol{u} = \delta\alpha\,{}^1\boldsymbol{u} + \delta\boldsymbol{w} \tag{2.38} $$

Here $\delta\alpha$ is an arbitrary scalar and $\delta\boldsymbol{w}$ is an arbitrary displacement field orthogonal to ${}^1\boldsymbol{u}$ in the same manner as ${}^2\boldsymbol{u}$, ${}^3\boldsymbol{u}$, ... Inserting this in the second order problem, ${}^2\boldsymbol{u}$ and a can be determined, and similarly ${}^3\boldsymbol{u}$ and b are determined from the third order problem. By substituting Eq. (2.38) into the reduced second order problem it is separated into a part used to determine the a-factor and a part used to determine ${}^2\boldsymbol{u}$.

$$ \begin{aligned} &\delta\alpha \underbrace{\left[\lambda_c{}^0\boldsymbol{\sigma} \cdot l_{11}\left({}^2\boldsymbol{u}, {}^1\boldsymbol{u}\right) + \left(a\lambda_c{}^0\boldsymbol{\sigma} + {}^1\boldsymbol{\sigma}\right) \cdot l_{11}\left({}^1\boldsymbol{u}, {}^1\boldsymbol{u}\right) + {}^2\boldsymbol{\sigma} \cdot l_1\left({}^1\boldsymbol{u}\right)\right]}_{\text{Used to determine } a} \\ &+ \underbrace{\left[\lambda_c{}^0\boldsymbol{\sigma} \cdot l_{11}\left({}^2\boldsymbol{u}, \delta\boldsymbol{w}\right) + \left(a\lambda_c{}^0\boldsymbol{\sigma} + {}^1\boldsymbol{\sigma}\right) \cdot l_{11}\left({}^1\boldsymbol{u}, \delta\boldsymbol{w}\right) + {}^2\boldsymbol{\sigma} \cdot l_1\left(\delta\boldsymbol{w}\right)\right]}_{\text{Used to determine } {}^2\boldsymbol{u}} = 0 \end{aligned} \tag{2.39} $$

Each part of the equation must equate to zero in order to be able to select $\delta\alpha$ and $\delta\boldsymbol{w}$ arbitrarily. From the first bracket the a-factor can be determined. The orthogonality condition ${}^0\boldsymbol{\sigma} \cdot l_{11}\left({}^1\boldsymbol{u}, {}^2\boldsymbol{u}\right) = 0$ is applied hereby eliminating the first term. The last term includes the undetermined second post-buckling stress, ${}^2\boldsymbol{\sigma}$ which is a function of ${}^2\boldsymbol{u}$. To eliminate ${}^2\boldsymbol{u}$ the following identity is used

$$ \begin{aligned} {}^2\boldsymbol{\sigma} \cdot l_1\left({}^1\boldsymbol{u}\right) &= {}^2\boldsymbol{\sigma} \cdot {}^1\boldsymbol{\epsilon} = {}^1\boldsymbol{\sigma} \cdot {}^2\boldsymbol{\epsilon} = {}^1\boldsymbol{\sigma} \cdot \left(l_1\left({}^2\boldsymbol{u}\right) + \frac{1}{2} l_2\left({}^1\boldsymbol{u}\right)\right) \\ &= \frac{1}{2}\,{}^1\boldsymbol{\sigma} \cdot l_2\left({}^1\boldsymbol{u}\right) \end{aligned} \tag{2.40} $$

Here the orthogonality condition ${}^1\boldsymbol{\sigma} \cdot l_1\left({}^2\boldsymbol{u}\right) = 0$ is applied. The first identity can be realized by switching to index notation and noting that ${}^2\sigma_{ij} = C_{ijkl}\,{}^2\epsilon_{kl}$ thus

$$ {}^2\sigma_{ij}\,{}^1\epsilon_{ij} = C_{ijkl}\,{}^2\epsilon_{kl}\,{}^1\epsilon_{ij} $$

Remembering from theory of elasticity that $C_{ijkl} = C_{klij}$ one obtain

$$ C_{ijkl}\,{}^2\epsilon_{kl}\,{}^1\epsilon_{ij} = C_{klij}\,{}^2\epsilon_{kl}\,{}^1\epsilon_{ij} = {}^2\epsilon_{kl}\,{}^1\sigma_{kl} = {}^2\boldsymbol{\epsilon} \cdot {}^1\boldsymbol{\sigma} $$

Inserting Eq. (2.40) into Eq. (2.39) the a-factor is determined as

$$a\lambda_c = -\frac{3}{2}\frac{{}^1\boldsymbol{\sigma}\cdot l_2\left({}^1\boldsymbol{u}\right)}{{}^0\boldsymbol{\sigma}\cdot l_2\left({}^1\boldsymbol{u}\right)} \tag{2.41}$$

In the second part of Eq. (2.39) $a\lambda_c{}^0\boldsymbol{\sigma}\cdot l_{11}\left({}^1\boldsymbol{u},\delta\boldsymbol{w}\right) = 0$ because $\delta\boldsymbol{w}$ possesses the same orthogonality properties as the ${}^p\boldsymbol{u}$ displacement fields. The ${}^1\boldsymbol{\sigma}\cdot l_{11}\left({}^1\boldsymbol{u},\delta\boldsymbol{w}\right)$-term is non-zero, as the orthogonality is defined through the pre-buckling stress field, whereas this term consist of post-buckling terms. By rearranging the equation, the second post-buckling displacement field is determined

$${}^2\boldsymbol{\sigma}\cdot l_1\left(\delta\boldsymbol{u}\right) + \lambda_c{}^0\boldsymbol{\sigma}\cdot l_{11}\left({}^2\boldsymbol{u},\delta\boldsymbol{u}\right) = -{}^1\boldsymbol{\sigma}\cdot l_{11}\left({}^1\boldsymbol{u},\delta\boldsymbol{u}\right) \tag{2.42}$$

By comparison to Eq. (2.37) the left hand side is singular and the right hand side represents a pseudo load vector. The equation can be solved with the constraint that ${}^2\boldsymbol{u}$ is orthogonal to ${}^1\boldsymbol{u}$ such that a definite system is obtained.

In the third order problem only the b-factor is of interest when determining whether the initial post-buckling response is stable or unstable, see Figure 2.6. Inserting $\delta\boldsymbol{u}$ from Eq. (2.38) into the third order problem, the equation is separated into a part used to determine b and a part used to determine ${}^3\boldsymbol{u}$ in the same manner as Eq. (2.41)

$$\begin{aligned}
&\delta\alpha\left[\lambda_c{}^0\boldsymbol{\sigma}\cdot l_{11}\left({}^3\boldsymbol{u},{}^1\boldsymbol{u}\right) + {}^3\boldsymbol{\sigma}\cdot l_1\left({}^1\boldsymbol{u}\right) + \left(a\lambda_c{}^0\boldsymbol{\sigma} + {}^1\boldsymbol{\sigma}_1\right)\cdot l_{11}\left({}^2\boldsymbol{u},{}^1\boldsymbol{u}\right)\right]\\
&+\delta\alpha\left[\left(b\lambda_c{}^0\boldsymbol{\sigma} + {}^2\boldsymbol{\sigma}\right)\cdot l_{11}\left({}^1\boldsymbol{u},{}^1\boldsymbol{u}\right)\right]\\
&+\left[\lambda_c{}^0\boldsymbol{\sigma}\cdot l_{11}\left({}^3\boldsymbol{u},\delta\boldsymbol{w}\right) + {}^3\boldsymbol{\sigma}\cdot l_1\left(\delta\boldsymbol{w}\right) + \left(a\lambda_c{}^0\boldsymbol{\sigma} + {}^1\boldsymbol{\sigma}_1\right)\cdot l_{11}\left({}^2\boldsymbol{u},\delta\boldsymbol{w}\right)\right]\\
&+\left(b\lambda_c{}^0\boldsymbol{\sigma} + {}^2\boldsymbol{\sigma}\right)\cdot l_{11}\left({}^1\boldsymbol{u},\delta\boldsymbol{w}\right) = 0
\end{aligned} \tag{2.43}$$

Again $\delta\alpha$ and $\delta\boldsymbol{w}$ can be selected arbitrary, thus each coefficient must equate to zero. Since only the b-factor is of interest the $\delta\alpha$ term is considered

$$\begin{aligned}
&\lambda_c{}^0\boldsymbol{\sigma}\cdot l_{11}\left({}^3\boldsymbol{u},{}^1\boldsymbol{u}\right) + {}^3\boldsymbol{\sigma}\cdot l_1\left({}^1\boldsymbol{u}\right) + \left(a\lambda_c{}^0\boldsymbol{\sigma} + {}^1\boldsymbol{\sigma}_1\right)\cdot l_{11}\left({}^2\boldsymbol{u},{}^1\boldsymbol{u}\right)\\
&+\left(b\lambda_c{}^0\boldsymbol{\sigma} + {}^2\boldsymbol{\sigma}\right)\cdot l_{11}\left({}^1\boldsymbol{u},{}^1\boldsymbol{u}\right) = 0
\end{aligned} \tag{2.44}$$

The idea is now to apply a similar approach as when the a-factor is determined. Due to orthogonality, $\lambda_c{}^0\boldsymbol{\sigma}\cdot l_{11}\left({}^3\boldsymbol{u},{}^1\boldsymbol{u}\right) = a\lambda_c{}^0\boldsymbol{\sigma}\cdot l_{11}\left({}^2\boldsymbol{u},{}^1\boldsymbol{u}\right) = 0$. To eliminate the unknown stress ${}^3\boldsymbol{\sigma}$ the same approach as used to eliminate ${}^2\boldsymbol{\sigma}$ in Eq. (2.40) is applied. From this ${}^3\boldsymbol{\sigma}\cdot{}^1\boldsymbol{\epsilon} = {}^1\boldsymbol{\sigma}\cdot l_{11}\left({}^1\boldsymbol{u},{}^2\boldsymbol{u}\right)$, and the b-factor is determined as

$$b\lambda_c = -\frac{{}^2\boldsymbol{\sigma}\cdot l_2\left({}^1\boldsymbol{u}\right) + 2{}^1\boldsymbol{\sigma}_1\cdot l_{11}\left({}^1\boldsymbol{u},{}^2\boldsymbol{u}\right)}{{}^0\boldsymbol{\sigma}\cdot l_2\left({}^1\boldsymbol{u}\right)} \tag{2.45}$$

Note that the denominators between the two Koiter factors are equal.

The Budiansky-Hutchinson notation can be translated into finite element notation by using Table 2.1. To have a notation consistent with the one used in Paper C, the nodal displacements are termed **U** instead of **D**. This translation can be obtained by comparing the governing finite element equations and the equations derived above.

Table 2.1: Translation between the Budiansky-Hutchinson notation and finite element notation. $\mathbf{B}_0$ and $\mathbf{B}_L$ are the linear and nonlinear element strain-displacement matrices, respectively, $\mathbf{E}$ is the constitutive matrix, $\mathbf{U}$ and $\mathbf{V}$ are the global nodal displacements, and $\mathbf{U}^e$ and $\mathbf{V}^e$ are element nodal displacements.

Term	Budiansky-Hutchinson	Finite element
	$l_1(\boldsymbol{u})$	$\mathbf{B}_0\mathbf{U}^e$
	$l_2(\boldsymbol{u})$	$\mathbf{B}_L(\mathbf{U}^e)\mathbf{U}^e$
	$l_{11}(\boldsymbol{u},\boldsymbol{v})$	$\mathbf{B}_L(\mathbf{U}^e)\mathbf{V}^e$
${}^0\epsilon$	$l_1\left({}^0\boldsymbol{u}\right)$	$\mathbf{B}_0{}^0\mathbf{U}^e$
${}^1\epsilon$	$l_1\left({}^1\boldsymbol{u}\right)$	$\mathbf{B}_0{}^1\mathbf{U}^e$
${}^2\epsilon$	$l_1\left({}^2\boldsymbol{u}\right)+\frac{1}{2}l_2\left({}^1\boldsymbol{u}\right)$	$\mathbf{B}_0{}^2\mathbf{U}^e+\frac{1}{2}\mathbf{B}_L\left({}^1\mathbf{U}^e\right){}^1\mathbf{U}^e$
σ	$H(\boldsymbol{\epsilon})$	$\mathbf{E}\epsilon$

The zeroth and first order problems are given by Eq. (2.4) and (2.11), respectively, thus no more attention is paid to those. The second order problem to obtain ${}^2\mathbf{U}$ is given by

$$\begin{bmatrix} \mathbf{K}_0+\lambda_c\mathbf{K}_\sigma^0 & \mathbf{K}_0{}^1\mathbf{U} \\ \left({}^1\mathbf{U}\right)^T\mathbf{K}_0 & -\varepsilon \end{bmatrix}\begin{Bmatrix} {}^2\mathbf{U} \\ \mu \end{Bmatrix}=\begin{Bmatrix} -\left(\mathbf{K}_\sigma^1+\frac{1}{2}\mathbf{K}_{0L}\right){}^1\mathbf{U} \\ 0 \end{Bmatrix} \tag{2.46}$$

Here the superscript before $\mathbf{U}$ defines the displacement field in the expansion, $\mathbf{K}_\sigma^0$ and $\mathbf{K}_\sigma^1$ are the stress stiffness matrices formulated on the pre-buckling displacement field and the first buckling mode shape, respectively. $\mathbf{K}_{0L}$ is an unsymmetric matrix given as

$$\mathbf{K}_{0L}=\sum_e^{n^e}\int_{V_e}\mathbf{B}_0^T\mathbf{E}\mathbf{B}_L\left({}^1\mathbf{U}^e\right)\mathrm{d}V \tag{2.47}$$

Here the summation over all elements involves assembly to global level, $\mathbf{B}_0$ is the linear element strain displacement matrix, $\mathbf{E}$ is the element constitutive matrix, $\mathbf{B}_L\left({}^1\mathbf{U}^e\right)$ is the element nonlinear strain-displacement matrix constructed using the buckling mode shape, V_e is the element volume, and n^e is the number of finite elements. The orthogonality condition is imposed using a perturbed Lagrangian approach, and the resulting system of equations is non-singular. Different values of the penalization parameter, ε, have been tested, and it did not show any effect on the final results, thus a penalization of 1 is chosen. Furthermore, following the approach proposed in [53], where λ_c has been perturbed by a parameter close to but smaller than 1 did not provide any numerical advantages over Eq. (2.46). The Koiter factors are most effectively

calculated using element summations, and they are given as

$$a\lambda_c = -\frac{3}{2}\sum_{e=1}^{n^e}\frac{\int_{V_e} {}^1\boldsymbol{\sigma}^T\mathbf{B}_L\left({}^1\mathbf{U}^e\right)\,\mathrm{d}V\,{}^1\mathbf{U}^e}{\int_{V_e} {}^0\boldsymbol{\sigma}^T\mathbf{B}_L\left({}^1\mathbf{U}^e\right)\,\mathrm{d}V\,{}^1\mathbf{U}^e} \tag{2.48}$$

$$b\lambda_c = -\sum_{e=1}^{n^e}\frac{\int_{V_e} {}^2\boldsymbol{\sigma}^T\mathbf{B}_L\left({}^1\mathbf{U}^e\right)\,\mathrm{d}V\,{}^1\mathbf{U}^e + 2\int_{V_e} {}^1\boldsymbol{\sigma}^T\mathbf{B}_L\left({}^1\mathbf{U}^e\right)\,\mathrm{d}V\,{}^2\mathbf{U}^{e\,e}}{\int_{V_e} {}^0\boldsymbol{\sigma}^T\mathbf{B}_L\left({}^1\mathbf{U}^e\right)\,\mathrm{d}V\,{}^1\mathbf{U}} \tag{2.49}$$

These equations can be used to implement Koiter asymptotic analysis with general isoparametric elements. The Koiter analysis comes with some important properties:

- The nonlinear post-buckling equations are replaced by a series of much simpler linear problems.
- The higher order problems depend on the lower order problems but not vice versa.
- If a better representation of the post-buckling response is needed one can add additional terms into the expansion. The cost is roughly an additional linear analysis.
- The computational cost of performing a two term Koiter analysis is approximately one buckling analysis and one linear static analysis.
- The stability of the structure is determined by the Koiter factors which makes it easy to evaluate the post-buckling stability compared to a full GNL analysis. If a structure is subjected to several load cases, then Koiter analysis is an effective method to determine the load cases of interest which should be subject to a more detailed GNL analysis.

2.7 Post-buckling optimization

Often a structure is designed such that buckling does not occur during operation. Analyzing the post-buckling response will reveal whether the structure is capable of carrying more load in the buckled configuration, which may be the case in overload situations, and if the structure is sensitive towards imperfections. Buckling of a structure results in a load redistribution throughout the structure which may or may not be catastrophical. To be able to push the design load closer to the buckling load it is important to design a structure which is capable of operating in a buckled configuration.

When performing post-buckling optimization it is important to apply the correct post-buckling optimization criteria. Considering a plate one may formulate the post-buckling optimization criteria based on the inplane properties like compliance, end-shortening, end-strain etc., or the out-of-plane properties like out-of-plane deflection. The optimum for one criterion is not necessarily the optimum for the other [58, 59]. The displacements emerging from buckling can be critical if:

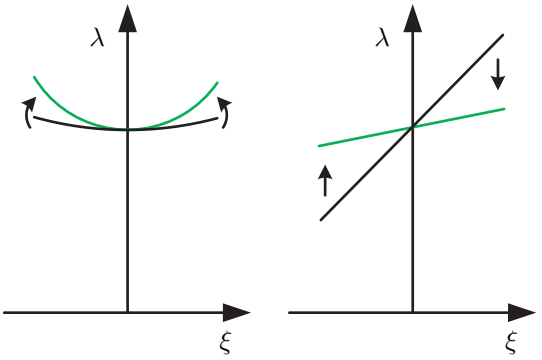

Figure 2.7: Sketch of the considered post-buckling stability optimization criteria. Green defines the optimized response and black the initial response. The left figure displays a maximization of the post-buckling curvature, whereas the right figure is a minimization of the asymmetry in the post-buckling response.

- The structure must have a shape close to the pre-buckled to perform optimally. This can be the case if an aerodynamic shape is required.
- Especially for stiffened panels: the buckled shape can induce a displacement field resembling a mode I crack, which can cause skin-stiffener separation.

Out-of-plane deflection has been observed to cause failure of wind turbine blades. An example is given in [60] where the blade failed because of skin buckling and subsequent delamination between the skin and main spar.

In this work post-buckling optimization is attempted based on asymptotic analysis and gradient based design optimization in Paper C. If the asymptotic post-buckling analysis is applied the optimization can be formulated based on the Koiter factors. Optimization using asymptotic approximations of the post-buckling response has previously been conducted in [61, 62]. Considering the Koiter asymptotic expansion two different optimization criteria can be formulated relating to the load factor expansion. With reference to Figure 2.7 the optimizations either consider maximization of the curvature or minimization of the asymmetry in the load factor expansion. Defining post-buckling stability as the resistance towards evolution of the buckled shape, then maximization of the post-buckling curvature is equivalent to maximization of the post-buckling stability of the structure considering symmetric post-buckling. Since asymmetric buckling always is unstable, minimization of the asymmetry can be used to obtain a symmetric response which then can be subjected to a secondary optimization making the structure post-buckling stable.

Chapter 3

Summary of results and concluding remarks

This chapter serves as an introduction to the included papers. Initially a summary of each paper is given highlighting the objectives, approaches, and conclusions. Afterwards, a summary of the contributions and the impact of the work is presented. Lastly, recommendations and directions for future research are given.

3.1 Description and conclusions of the papers

In this chapter a summary of the papers is given. The papers constitute the basis for the contributions obtained during the PhD project.

3.1.1 Paper A

In the paper a method for stiffness optimization of laminated composite structures is developed. The optimization is formulated on basis of Free Material Optimization, and the commercially available finite element analysis software ANSYS is used to evaluate the structural response. This is chosen to avoid the use of specialized analysis and design optimization codes and to demonstrate the applicability of optimization in conjunction with commercially available finite element analysis software. To avoid the use of finite differences and stochastic search methods, the optimality criterion approach and heuristic update scheme from [26] are used to optimize the structures. The Free Material Optimization formulation is extended to accommodate commercially available finite element analysis codes and shell elements. To enhance manufacturability a patch formulation is derived which decouples the material and finite element discretizations, and secure a minimum length scale in the final design. Laminated composite materials rarely consist of a single ply, hence a multi-layered Free Material Optimization is formulated to enable the optimization of laminated materials. The optimization procedure is demonstrated on two

examples; the clamped-clamped plate with two load cases from [10] and the square doubly curved corner hinged shell from [15].

The first example is used to demonstrate both a multiple load case example and the effect of including patches of various size. The optimized structures from Free Material Optimization are compared to those from Discrete Material Optimization and Continuous Fiber Angle Optimization using a sequential linear programming algorithm. Good correlation exists between the different optimization procedures. For the Free Material Optimization formulation it is observed that increasing the patch size results in a material which possess more bi-directional constitutive properties. This is because the individual patches must span a larger part of the strain field, which increases the possibility of variations in the strains within the individual patches. Consequently, the optimum material must possess stiffness in more directions compared to a finer patch discretization.

The advantage of a multilayered free material formulation is demonstrated in the second example. The optimized shell is a complex sandwich structure where each individual layer has a unique topology and set of fiber angles. The obtained layered structure would be difficult or impossible to interpret from a single layered model. The results from Free Material Optimization are compared to those from Discrete Material Optimization and good correlation in the topology and fiber angles is obtained.

In conclusion, the paper demonstrates the applicability of Free Material Optimization implemented within a commercial environment to obtain optimal designs of laminated composite structures.

3.1.2 Paper B

The second paper follows up on the work in [32] and further develops the recurrence optimization approach for robust buckling optimization of laminated composite structures. Furthermore, a Discrete Material Optimization formulation for nonlinear buckling analysis is formulated. It is combined with "worst" shape imperfection optimization to obtain robust buckling optimal structures. In the recurrence optimization either the laminate is optimized for a geometrically imperfect structure, hereby maximizing the buckling load, or for a given laminate layup, the geometric imperfection which minimizes the buckling load is determined. The optimization problems are solved in a sequential manner until convergence. A new evaluation of the imperfection sensitivity is formulated, where the imperfection sensitivity is defined as the difference in buckling load between the perfect structure and the structure with the "worst" shape imperfection imposed. A common basis for comparison of the laminate designs is obtained. The framework enables the possibility to monitor the imperfection sensitivity throughout the optimization, and the effect of the optimization on the upper bound (perfect) performance is clarified.

To secure a consistent penalization between the tangential stiffness matrix, internal forces, and the nonlinear buckling problem in the Discrete Material Optimization, the same penalization is used for $\mathbf{K}_0$, $\mathbf{K}_L$, and $\mathbf{K}_S$. Since the

same penalization is applied for all stiffness terms, one might expect convergence problems. Throughout the paper it is demonstrated that convergence is not an issue when having the same penalization. The "worst" shape imperfection optimization is parameterized using the lowest linear buckling mode shapes as these are easily obtained and provide an orthogonal basis for the optimization.

A laminated composite U-profile and a cylindrical panel are used to demonstrate the optimization. The U-profile buckles with a limit point instability, where no mode switching is observed during the optimization. The cylindrical panel buckles with a bifurcation instability, and the four lowest buckling loads are located within 1%, thus mode switching is expected during the optimization. For both cases the imperfection sensitivity is decreased, as the recurrence optimization is performed. Even though mode switching is present during the optimization, the recurrence optimization converges, with the cost of more iterations compared to the cases where mode switching does not occur. For both examples the imperfect buckling load is increased during the optimization, while the imperfection sensitivity is decreased. Thus buckling optimal designs which are less sensitive towards imperfections are obtained.

To sum up, this paper demonstrates a framework for robust buckling optimization of laminated composite structures. Robustness is defined through the imperfection sensitivity, where a new formulation for evaluating the imperfection sensitivity is presented.

3.1.3 Paper C

In this paper a novel method for gradient based post-buckling optimization of laminated composite structures is developed. The optimization is based on asymptotic post-buckling analysis assuming a linear pre-buckling state and simple (distinct) buckling load factors. The design sensitivities for the Koiter a and b-factors and the associated displacement fields are derived in order to perform gradient based optimization.

The paper discusses different choices of optimization formulations when optimizing the post-buckling response, and it is demonstrated that optimal structures for one criteria are not necessarily optimal for other post-buckling criteria. Post-buckling stability is defined as the resistance towards evolution of a buckle, and the more stable the post-buckling response the higher load is needed.

Different optimization formulations are developed. The new objectives and constraints are based on the Koiter factors, and they are used to demonstrate the proposed method. These criterion functions are formulated to maximize the stability or in the case of an asymmetric post-buckling response, minimize the asymmetry of the response hereby obtaining a more symmetric post-buckling response.

The proposed optimization formulations are demonstrated on a single layered simply supported square plate and an 8 layered simply supported cylindrical panel. The plate represents an example which exhibits symmetric post-

buckling whereas the cylindrical panel has an asymmetric post-buckling response. The proposed methods successfully maximize the post-buckling stability of the structures and minimize the asymmetry in the asymptotic post-buckling response. Furthermore, for both examples the dependency between the buckling load and the post-buckling response is demonstrated. Generally speaking, by optimizing the post-buckling stability the buckling load is decreased and vise versa. In the paper, the effects of constraining either the Koiter parameters or the buckling load factors are demonstrated. Additionally, it is demonstrated how to obtain post-buckling optimal designs which possess a high buckling load with the use of asymptotic post-buckling analysis.

In conclusion, this paper presents a novel method for gradient based post-buckling optimization of laminated composite structures. The design sensitivities for the Koiter factors are derived within this work. Formulations for post-buckling optimization are developed and demonstrated to provide post-buckling optimum structures.

3.2 Contributions and impact

The work presented in the thesis focuses on developing optimization methods for laminated composite structures. Three different topics have been addressed throughout the thesis, namely stiffness optimization using Free Material Optimization, robust buckling optimization using Discrete Material Optimization and "worst" shape imperfection, and lastly post-buckling optimization using Continuous Fiber Angle Optimization.

The methods formulated in Paper B and C, although applied to laminated composite structures, are derived in a general sense, and thus can be used with other kinds of material parameterizations and for other kinds of structures e.g., metallic structures.

The first steps towards applying free material optimization in a commercial context have been performed in this work. This demonstrates the potential for application of Free Material Optimization in industry. A multilayered Free Material Optimization formulation is derived within this work that allows interpretation of a multilayered laminated composite structure which otherwise remain hidden in the single layer Free Material Optimization formulation.

Manufacturability of free material optimized structures has been enhanced by the introduction of a patch formulation which forces larger areas of a structure to have the same material properties.

Paper B extends the Discrete Material Optimization approach to structures exhibiting nonlinear response, more precisely nonlinear buckling and geometrically nonlinear static analysis. It is demonstrated that applying the same penalization on all stiffness terms provides a consistent penalization of the

static and buckling problems without convergence issues.

Manufacturable robust buckling design optimization of laminated composite structures is demonstrated by combining the Discrete Material Optimization approach with the "worst" shape imperfection optimization approach. Here the laminate layup consist of fibers aligned at standard angles, and by optimizing the "worst" imperfect structure manufacturable imperfection insensitive structures are obtained.

Normally when robust design is conducted only the performance of the imperfect structure is considered when evaluating the imperfection sensitivity. Paper B provides a new interpretation of imperfection sensitivity which can be used to compare structures with different laminate layup. This is enabled by using the perfect structure as basis for comparison together with the "worst" shape imperfect structure.

In Paper C a novel post-buckling optimization formulation is derived. The optimization method combines asymptotic post-buckling analysis with a gradient based optimization method to obtain post-buckling optimal structures. Formulations which handle both asymmetric post-buckling and symmetric post-buckling responses are developed and demonstrated.

The design sensitivities for asymptotic post-buckling optimization are derived using the direct differentiation method. The derivation is performed in a general manner to enable the use of different parameterizations. Demonstration of the gradient based optimization is conducted using Continuous Fiber Angle Optimization, but other laminate parameterizations like the Discrete Material Optimization parameterization can be implemented within the presented framework.

The proposed post-buckling optimization successfully optimizes the post-buckling stability even though the pre-buckling response is nonlinear, resulting in structures with increased post-buckling stability.

The post-buckling optimization method operates directly on the physical phenomenon related to post-buckling stability. Other post-buckling optimization formulations e.g., nonlinear compliance at a post-buckling configuration do not operate directly on the physics controlling the post-buckling response. Consequently, the proposed method enables the possibility of obtaining a better performance of the structure in the post-buckling regime.

3.3 Perspectives and future work

The research conducted during the PhD project naturally leads to new topics to be pursued in the future. These are summarized for each paper individually.

Paper A demonstrates stiffness design using commercially available finite element analysis codes using a free material parameterization. As free material optimized designs do not represent a physical material, a method to determine the optimum physical material from the free material is needed. Furthermore, stiffness optimal designs are not optimum in all cases, thus new formulations which effectively handle other design criteria like strength, buckling, eigenfrequency, mass etc., in combination with commercially available finite element analysis software are needed.

Paper B combines the Discrete Material Optimization and "worst" shape imperfection optimization approaches to perform robust design optimization. However, when increasing the penalization for the Discrete Material Optimization problem care must be taken to secure that the structural response remains similar before and after the change in penalization. Because of that, new penalization strategies should be developed which secure that sufficient stiffness remains after penalization. This can also be exploited in standard topology optimization. The recurrence optimization approach has only been demonstrated for cases where the laminate and shape optimizations are performed until convergence before the next recurrence optimization iteration is performed. This approach can be time consuming if several recurrence optimization iterations are required. To reduce the total optimization time it might be possible to switch between the two optimizations after a fixed number of iterations, but comparative studies to the current approach are needed to validate the suggested change.

Paper C develops a novel gradient based optimization method based on asymptotic post-buckling analysis. The design sensitivities have been derived in a general manner, but the optimization formulations need to be demonstrated with other parameterizations like Discrete Material Optimization. Furthermore, formulations which can handle mode switching in the post-buckling regime and effectively optimize the structure under these circumstances are needed. In the current formulation an asymmetric post-buckling response is minimized subject to a curvature constraint. It may be advantageous to consider a combined optimization formulation, where the optimum combination between the post-buckling asymmetry and curvature is determined, hereby allowing a slightly larger post-buckling asymmetry with the effect of a significantly increased post-buckling curvature. A comparison study with other post-buckling optimization formulations can reveal the effectiveness and further properties of the proposed method. The optimization has been demonstrated on simple structures, and to demonstrate the general applicability of the method, general structures with possible nonlinear pre-buckling response should be optimized. This also requires that the derived sensitivities are extended to the nonlinear case.

References

[1] Jones RM. *Mechanics of composite materials*. 2nd edn., Materials Science and Engineering Series, Taylor & Francis Group, 1999.

[2] Kassapoglou C. *Design and Analysis of Composite Structures: With Applications to Aerospace Structures*. Aerospace Series, Wiley, 2011.

[3] Bažant ZP, Cedolin L. *Stability of Structures: Elastic, Inelastic, Fracture and Damage Theories*. World Scientific, 2010.

[4] Ghiasi H, Pasini D, Lessard L. Optimum stacking sequence design of composite materials Part I: Constant stiffness design. *Composite Structures* 2009; **90**(1):1–11.

[5] Ghiasi H, Fayazbakhsh K, Pasini D, Lessard L. Optimum stacking sequence design of composite materials Part II: Variable stiffness design. *Composite Structures* 2010; **93**(1):1–13.

[6] Pedersen P. On optimal orientation of orthotropic materials. *Structural optimization* 1989; **1**(2):101–106.

[7] Pedersen P. Bounds on elastic energy in solids of orthotropic materials. *Structural optimization* 1990; **2**(1):55–63.

[8] Ringertz U. On finding the optimal distribution of material properties. *Structural optimization* 1993; **5**(4):265–267.

[9] Bendsøe MP, Guedes JM, Haber RB, Pedersen P, Taylor JE. An Analytical Model to Predict Optimal Material Properties in the Context of Optimal Structural Design. *Journal of Applied Mechanics* 1994; **61**(4):930–937.

[10] Bendsøe MP, Díaz AR, Lipton R, Taylor JE. Optimal design of material properties and material distribution for multiple loading conditions. *International Journal for Numerical Methods in Engineering* 1995; **38**(7):1149–1170.

[11] Bendsøe MP, Guedes JM, Plaxton S, Taylor JE. Optimization of structure and material properties for solids composed of softening material. *International Journal of Solids and Structures* 1996; **33**(12):1799–1813.

[12] Kočvara M, Stingl M, Zowe J. Free material optimization: recent progress†. *Optimization* 2008; **57**(1):79–100.

[13] Hörnlein H, Kočvara M, Werner R. Material optimization: bridging the gap between conceptual and preliminary design. *Aerospace Science and Technology* 2001; **5**(8):541–554.

[14] Sigmund O, Torquato R. Design of materials with extreme thermal expansion using a three-phase topology optimization method. *Journal of the Mechanics and Physics of Solids* 1997; **45**(6):1037–1067.

[15] Stegmann J, Lund E. Discrete material optimization of general composite shell structures. *International Journal for Numerical Methods in Engineering* 2005; **62**(14):2009–2027.

[16] Lund E, Stegmann J. On structural optimization of composite shell structures using a discrete constitutive parametrization. *Wind Energy* 2005; **8**(1):109–124.

[17] Hvejsel CF, Lund E, Stolpe M. Optimization strategies for discrete multi-material stiffness optimization. *Structural and Multidisciplinary Optimization* 2011; **44**(2):149–163.

[18] Hvejsel CF, Lund E. Material interpolation schemes for unified topology and multi-material optimization. *Structural and Multidisciplinary Optimization* 2011; **43**(6):811–825.

[19] Bendsøe M, Sigmund O. *Topology Optimization: Theory, Methods and Applications*. 2nd edn., Springer-Verlag, Berlin, 2003.

[20] Rietz A. Sufficiency of a finite exponent in SIMP (power law) methods. *Structural and Multidisciplinary Optimization* 2001; **21**:159–163.

[21] Stolpe M, Svanberg K. An alternative interpolation scheme for minimum compliance topology optimization. *Structural and Multidisciplinary Optimization* 2001; **22**:116–124.

[22] Lund E. Buckling topology optimization of laminated multi-material composite shell structures. *Composite Structures* 2009; **91**(2):158–167.

[23] Sørensen S, Sørensen R, Lund E. DMTO - a method for Discrete Material and Thickness Optimization of laminated composite structures. *Structural and Multidisciplinary Optimization* 2014; **50**(1):25–47.

[24] Bruyneel M. SFP-a new parameterization based on shape functions for optimal material selection: application to conventional composite plies. *Structural and Multidisciplinary Optimization* 2011; **43**(1):17–27.

[25] Gao T, Zhang W, Duysinx P. A bi-value coding parameterization scheme for the discrete optimal orientation design of the composite laminate. *International Journal for Numerical Methods in Engineering* 2012; **91**(1):98–114.

[26] Pedersen P, Pedersen NL. On strength design using free material subjected to multiple load cases. *Structural and Multidisciplinary Optimization* 2013; **47**(1):7–17.

[27] Thompson J, Hunt G. *A General Theory of Elastic Stability*. Wiley, 1973.

[28] Brendel B, Ramm E. Linear and nonlinear stability analysis of cylindrical shells. *Computers & Structures* 1980; **12**(4):549–558.

[29] Riks E. An incremental approach to the solution of snapping and buckling problems. *International Journal of Solids and Structures* 1979; **15**(7):529–551.

[30] Crisfield MA. A fast incremental/iterative solution procedure that handles "snap-through". *Computers & Structures* 1981; **13**(1-3):55–62.

[31] Lindgaard E, Lund E. Nonlinear buckling optimization of composite structures. *Computer Methods in Applied Mechanics and Engineering* 2010; **199**(37-40):2319–2330.

[32] Lindgaard E, Lund E, Rasmussen K. Nonlinear buckling optimization of composite structures considering "worst" shape imperfections. *International Journal of Solids and Structures* 2010; **47**(22-23):3186–3202.

[33] Lindgaard E, Lund E. A unified approach to nonlinear buckling optimization of composite structures. *Computers & Structures* 2011; **89**(3-4):357–370.

[34] Lindgaard E, Lund E. Optimization formulations for the maximum nonlinear buckling load of composite structures. *Structural and Multidisciplinary Optimization* 2011; **43**(5):631–646.

[35] Lindgaard E, Dahl J. On compliance and buckling objective functions in topology optimization of snap-through problems. *Structural and Multidisciplinary Optimization* 2013; **47**(3):409–421.

[36] Lindgaard E. Buckling Optimization of Composite Structures. PhD Thesis, Department of Mechanical and Manufacturing Engineering, Aalborg University, Denmark 2010. Special report no. 69.

[37] Thompson J. Optimization as a generator of structural instability. *International Journal of Mechanical Sciences* 1972; **14**(9):627–629.

[38] Yao W, Chen X, Luo W, van Tooren M, Guo J. Review of uncertainty-based multidisciplinary design optimization methods for aerospace vehicles. *Progress in Aerospace Sciences* 2011; **47**(6):450 – 479.

[39] Deml M, Wunderlich W. Direct evaluation of the "worst" imperfection shape in shell buckling. *Computer Methods in Applied Mechanics and Engineering* 1997; **149**(1-4):201–222.

[40] Wunderlich W, Albertin U. Analysis and load carrying behaviour of imperfection sensitive shells. *International Journal for Numerical Methods in Engineering* 2000; **47**(1-3):255–273.

[41] El Damatty A, Nassef A. A finite element optimization technique to determine critical imperfections of shell structures. *Structural and Multidisciplinary Optimization* 2001; **23**(1):75–87.

[42] Kristanič N, Korelc J. Optimization method for the determination of the most unfavorable imperfection of structures. *Computational Mechanics* 2008; **42**(6):859–872.

[43] Bender CM, Orszag SA. *Advanced Mathematical Methods for Scientists and Engineers*. McGraw-Hill, 1978.

[44] Koiter WT. The stability of elastic equilibrium. PhD Thesis, Technische Hooge School Delft 1945. Translated by E. Riks.

[45] Byskov E. *Elementary Continuum Mechanics for Everyone*. 1st edn., Springer-Verlag, Berlin, 2013.

[46] Budiansky B. Theory of buckling and post-buckling behavior of elastic structures. *Advances in Applied Mechanics* 1974; **14**:1–65.

[47] Byskov E, Hutchinson W. Mode interaction in axially stiffened cylindrical shells. *AIAA Journal* 1977; **15**(7):941–948.

[48] Byskov E, Christensen CD, Jørgensen K. Elastic postbuckling with nonlinear constraints. *International Journal of Solids and Structures* 1996; **33**(17):2417–2436.

[49] Olesen JF, Byskov E. Accurate determination of asymptotic postbuckling stresses by the finite element method. *Computers & Structures* 1982; **15**(2):157–163.

[50] Arbocz J, Hol J. Koiter's stability theory in a computer-aided engineering (CAE) environment. *International Journal of Solids and Structures* 1990; **26**(9–10):945–973.

[51] Lanzo AD, Garcea G. Koiter's analysis of thin-walled structures by a finite element approach. *International Journal for Numerical Methods in Engineering* 1996; **39**(17):3007–3031.

[52] Garcea G, Madeo A, Zagari G, Casciaro R. Asymptotic post-buckling FEM analysis using corotational formulation. *International Journal of Solids and Structures* 2009; **46**(2):377–397.

[53] Rahman T, Jansen E. Finite element based coupled mode initial post-buckling analysis of a composite cylindrical shell. *Thin-Walled Structures* 2010; **48**(1):25–32.

[54] White S, Raju G, Weaver P. Initial post-buckling of variable-stiffness curved panels. *Journal of the Mechanics and Physics of Solids* 2014; **71**(0):132–155.

[55] Cochelin B, Damil N, Potier-Ferry M. Asymptotic-numerical methods and Pade approximants for non-linear elastic structures. *International Journal for Numerical Methods in Engineering* 1994; **37**(7):1187–1213.

[56] Vannucci P, Cochelin B, Damil N, Potier-Ferry M. An asymptotic-numerical method to compute bifurcating branches. *International Journal for Numerical Methods in Engineering* 1998; **41**(8):1365–1389.

[57] Shames I, Dym C. *Energy and Finite Element Methods In Structural Mechanics*. Si units edn., Taylor & Francis, 1996.

[58] Diaconu CG, Weaver PM. Approximate Solution and Optimum Design of Compression-Loaded, Postbuckled Laminated Composite Plates. *AIAA Journal* 2005; **43**(4):906–914.

[59] Diaconu CG, Weaver PM. Postbuckling of long unsymmetrically laminated composite plates under axial compression. *International Journal of Solids and Structures* 2006; **43**(22–23):6978–6997.

[60] Overgaard LCT, Lund E, Thomsen OT. Structural collapse of a wind turbine blade. part a: Static test and equivalent single layered models. *Composites Part A: Applied Science and Manufacturing* 2010; **41**(2):257 – 270.

[61] Raju G, White S, Wu Z, Weaver PM. Optimal Postbuckling Design of Variable Angle Tow Composites using Lamination Parameters. *Proceedings of 56th AIAA/ASCE/AHS/ASC Structures, Structural Dynamics, and Materials Conference*, American Institute of Aeronautics and Astronautics, 2015.

[62] White S, Weaver P. Towards Imperfection Insensitive Buckling Response of Shell Structures-Shells with Plate-like Post-buckled Responses. *Aeronautical Journal* 2015; 1–15; Accepted for publication July 2015.

SUMMARY

Laminated composite materials are widely used in the design of light weight high performance structures like wind turbine blades and aeroplanes due to their superior stiffness and strength-to-weight-ratios compared to their metal counter parts. Furthermore, the use of laminated composite materials allows for a higher degree of tailoring of the resulting material. To enable better utilization of the composite materials, optimum design procedures can be used to assist the engineer. This PhD thesis is focused on developing numerical methods for optimization of laminated composite structures.

The first part of the thesis is intended as an aid to read the included papers. Initially the field of research is introduced and the performed research is motivated. Secondly, the state-of-the-art is reviewed. The review includes parameterizations of the constitutive properties, linear and geometrically nonlinear analysis of structures, buckling and post-buckling analysis of structures, and formulations for optimization of structures considering stiffness, buckling, and post-buckling criteria. Lastly, descriptions, main findings, and conclusions of the papers are presented.

The papers forming the basis of the contributions of the PhD project are included in the second part of the thesis. Paper A presents a framework for free material optimization where commercially available finite element analysis software is used as analysis tool. Robust buckling optimization of laminated composite structures by including imperfections into the optimization process is the topic of Paper B. In Paper C the design sensitivities for asymptotic postbuckling optimization are derived. Furthermore, optimization formulations are introduced and demonstrated for optimum post-buckling design.

ISSN (online): 2246-1248
ISBN (online): 978-87-7112-408-8

AALBORG **UNIVERSITETSFORLAG**